



# Experimental and analytical study of an CF-PEEK Fastener all composites single-lap shear joint under static and fatigue loading

M. Schuett<sup>1</sup> · J. Karsten<sup>1</sup> · L. Schott<sup>1</sup> · H. Wittich<sup>1</sup> · K. Schulte<sup>1</sup> · B. Fiedler<sup>1</sup>

Received: 22 June 2018 / Revised: 22 September 2018 / Accepted: 6 October 2018 / Published online: 23 October 2018  
© Deutsches Zentrum für Luft- und Raumfahrt e.V. 2018

## Abstract

This paper presents a detailed experimental study on carbon fibre (CF) polyether etherketone (PEEK) composite fasteners designed to join conventional high performance composites (CFRP). The failure mechanisms of two CF-PEEK fasteners with countersunk heads joining two laminate plates in a single-lap configuration were investigated under static (tensile) and cyclic loading (tension–tension). The failure process of the bolted joints is described in detail using acoustic emission and microscopic cut views. For comparison the CF-PEEK fasteners were replaced by metal fasteners (Titanium) under the corresponding conditions and loadings. The experimental results are in good agreement with the newly developed “closed-form” model up to the damage point of the joints. This enhanced analytical approach is a closed-form extension of the spring-based method, where bolts and laminates are represented by an arrangement of springs and masses. The model covers in all variables influencing the joint behaviour, such as fastener position, joint material, fastener type, hole diameter, joint thickness, bolt-hole clearance, and bolt torque.

**Keywords** Single-lap shear joint · Mechanical testing · Acoustic emission · Spring method · Analytical model

## 1 Introduction

In the past decade, the civil aviation industry has seen breakthrough in the use of composite materials for passenger airplanes. Composites are favoured because of their low weight, high material stiffness and superior fatigue performance. The two market leaders Airbus and Boeing have introduced new aircraft models, as the A350 and the B787 respectively, which have their primary structure made from Carbon Fibre Reinforced Polymers (CFRP).

While materials have evolved, basic techniques used to fix/hold these structures together remain largely unchanged. In aircraft industry fasteners—made of steel or titanium—are widely used to join CFRP structures. Opposite to adhesive bonds they are removable and permit access to the interior of the structure for inspection or repair purposes.

However, the inevitable holes in the structural components lead to stress concentrations. Further, the large number of fasteners results in a weight penalty. Additionally, the

difference in the electrical potential conditions between the composite laminate and the metallic bolts results in galvanic corrosion. To overcome weight and corrosion problems of the metal fasteners, the idea of using fasteners made of composite materials arose.

In literature only few information can be found on CFRP fasteners. R. Starikov and J. Schön compared the quasi static and fatigue behaviour of titanium and composite fasteners. They found that titanium fasteners performed better under static loading, but under fatigue loading (up to  $10^6$  load cycles) both CFRP and titanium fasteners fail at about the same maximum stress level [1–4].

Reworked designs and production processes of the CF-PEEK-fasteners, suggest that the composite fastener has improved. This leads to a much wider field of application. Therefore, a deeper understanding of the failure mechanisms in static and fatigue loading is essential. Detailed investigations on composite bolted joints describe their failure processes in response to several key features such as clamping force, coefficient of friction, clearance/fitting tolerance, joint geometric details and laminate lay-up [5, 6].

In the bolted laminates microscopic failures can be detected at an early stage long before the finale fracture will occur. The failure process in quasi-static loading starts with

✉ M. Schuett  
martin.schuett@tuhh.de

<sup>1</sup> Institute of Polymers and Composites, Hamburg University of Technology, Hamburg, Germany

matrix cracking followed by fibre fracture in form of kink-bands in the laminate plates. When increasing the load on the joints, delaminations begin to extend from the borehole [7–9]. In addition, damages due to wear of the laminate surfaces around the area of the bolts are observed in fatigue loading [8, 10, 11].

Due to the eccentric loading of a single-lap joint, secondary bending is introduced into the joint, creating a non-uniform contact stress distribution between the bolt and the borehole edge. The result is a shear and tension force on the bolts [6]. For the failure of the CF-PEEK-fastener, three different failure modes can be detected due to the combined load case of shear and tension: Inter fibre failures in the contact area of the two laminate-plates, a shear of the countersunk head from the bolt and inter fibre fracture starting from the tooth flank after the first pitch [12–14]. The literature overview has shown that the failure process for composite bolted joints with steel or titanium fastener systems is already described in detail [15]. Based on these research results static and cyclic load tests with single-lap shear specimens are performed in this study, to describe the failure mechanisms of all CFRP-joint in detail.

For the design of bolted joints many design variables need to be considered. Variables which influence the joint behaviour are the fastener position, joint material, fastener type, hole diameter, joint thickness, bolt-hole clearance, and bolt torque.

Moreover, bolted joints represent areas with localized stress concentrations. Due to little stress relief by deformation around the holes, bolted composite joints can fail catastrophically upon extensive loading and tend to limit the structural integrity and load carrying capacity of an aircraft structure [16].

Design approaches determining the load distribution are often very conservative. Often numerical approaches are used to model the joint behaviour in detail, which easily becomes an ambitious problem [4]. We have addressed this problem by the expansion of an analytical method to give efficient design for all CFRP-joints. Tate and Rosenfeld [17] introduced a spring-based method to calculate the load distribution for double-lap joints with isotropic material properties for the fasteners. This method was extended by Nelson [18] to include anisotropic materials and single-lap joints into the calculation. Based on the analytical approaches of Tate and Rosenfeld, Nelson and Barrios [17–19], McCarthy [4, 16] and Liu [20] introduced a design optimization for the spring-based model of multi-bolt joints by taking torque and friction effects between the laminates and the bolt-hole clearance into account. A more detailed investigation on the influence of secondary bending is performed by Olmedo using a more complex analytical model [21].

Countersunk fasteners are of great interest for use in skin-structure joints where aerodynamic efficiency is important.

Single-lap joints mounted with countersunk fasteners result in a significant stress concentration and involve a highly complex stress distribution in the laminates [22–24]. Egan introduced a highly detailed analysis of the stress state for countersunk hole boundary, which studies the influence of the clearance on the stress state extensively [25].

For the optimization of bolted joints spring-based methods [16–18] are a very effective approach. In this study, an effective approach is presented to model the mechanical behaviour based on the current spring-based method [18]. Most of the main design variables are considered, with particular focus on implementing material properties and mechanical interaction between CF-PEEK-fastener and jointed CFRP laminates.

The acoustic emission (AE) method is employed to characterize the failure process. The AE investigations rely on the principle that events of certain failure modes create a defined acoustic signal. A literature review shows that three main techniques are basically used to characterise AE signals: (a) classification according to a signal parameter, (b) classification according to several parameters using pattern recognition techniques and (c) classification according to the extensional flexural mode content [26–31].

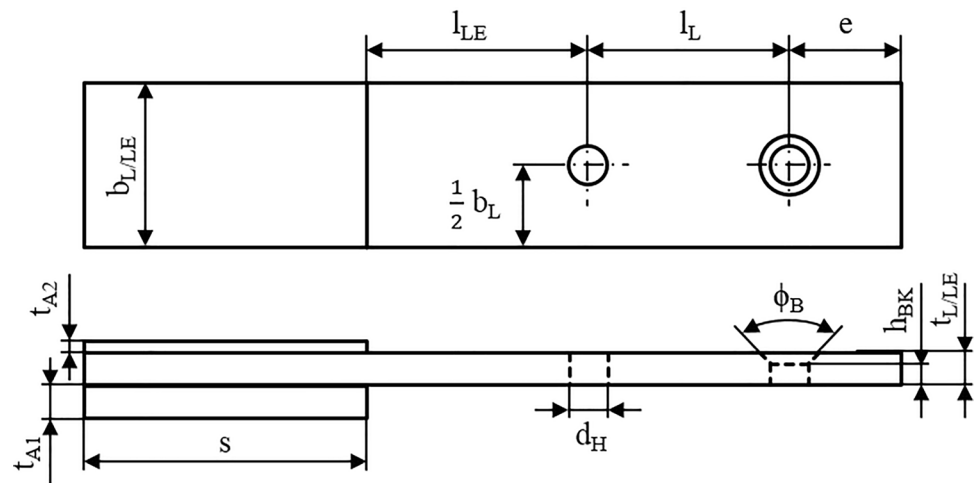
The AE-signals are collected from several standard single-lap-shear (SLS) tests with quasi-static and fatigue loading and analysed to get a more detailed view on the failure process of the bolted joint. First, the frequency content of the signals recorded in each test is analysed. Secondly, classifications of the failure process due to counts and true energy are correlated to the failure process.

## 2 Material and experimental procedure

### 2.1 Material and geometry

Single-lap shear (SLS) tests, based on ASTM D 5961 [32], are performed using specimens composed of two like halves fastened together through two centreline holes using two countersunk fasteners. The specimen half according to the drawing in Fig. 1, are composite plates consisting of a HEXCEL carbon fibre/epoxy material system (HexPly M21/35%/198/T800S) with quasi-isotropic layup [45/90/45/0]<sub>2S</sub>. The laminates are cured according the manufacturers recommendations in an autoclave process for 2 h at  $T = 180\text{ }^{\circ}\text{C}$  and a pressure of 5 bar. After curing all plates are proved to void free by ultrasonic C-scan. The nominal cured ply thickness of 0.19 mm was measured resulting in a total thickness of the CFRP-laminate of  $t_L = 3.04\text{ mm}$ . According to the standard, each specimen is mounted with two fasteners and the dimensions of the specimens are related to the diameter  $d_H$  of the borehole (see Fig. 1). The width of the each test specimens is set to  $b_L = 30\text{ mm}$ .

**Fig. 1** Geometry of specimen half for single-lap shear test with two fasteners according to ASTM D 5961 [32]



Jaws clamp the test specimen at its ends and apply the quasi-static and cyclic loads. Taps ensure an optimal load transmission into the specimens from the clamping system. A doubler to each grip avoids eccentric loading. The holes in the test specimens are drilled with countersink drillers from the company Klenk GmbH & Co. KG, Germany. They have a patented [33] fibre cracker on the drilling tool and distinct drilling parameters are used (driving speed 4000 1/min/feed 0.05 mm/ref), to minimize delamination, chip-out fibres and degradation of matrix due to overheating in the borehole edge.

In this work, three types of fasteners are tested consisting of bolt and nut:

- 1/4" CF-PEEK-bolt and -nut (IM7-fibre/PEEK-matrix) with countersunk head, shank diameter  $d=6.3$  mm, mass bolt  $M=0.99$  g, mass nut  $M=1.5$  g
- 3/16" CF-PEEK-bolt and -nut (IM7-fibre/PEEK-matrix) with countersunk head, shank diameter  $d=4.8$  mm, mass of bolt  $M=0.52$  g, mass nut  $M=0.53$  g

- 3/16" Titanium-bolt (Ti-6Al-4V) and steal-nut (302HQ) aerospace Hi-Lok series with countersunk head, shank diameter  $d=4.8$  mm, mass bolt  $M=1.1$  g, mass nut  $M=1.2$  g

The CF-PEEK-fastener systems for this study are manufactured in collaboration with the company icotec (Switzerland). Bolts and nuts are produced in a composite flow moulding process which is presented in detail by the work of Togni [34], addressed especially for this type of fastener. Detailed studies by Togni provide a good inside on the composite flow moulding process [34] and the mechanical properties of the CF-PEEK-fasteners [35, 36]. Mechanical properties of CF-PEEK fasteners are dependent on their internal architecture of the fibres. Whereas the fibre orientation of the out layers are affected by the contour of the fastener whereas the orientation of the inner layers is depended on the production process. The CF-PEEK fastener is divided into three category groups such as contour, transition and axially oriented fibres (see Fig. 2). In the area of the central axis, the fibres (white) are mainly axially oriented. In the

**Fig. 2** Fibre orientation of the CF-PEEK fasteners with three category groups contour oriented fibres, transition oriented fibres and axially oriented fibres

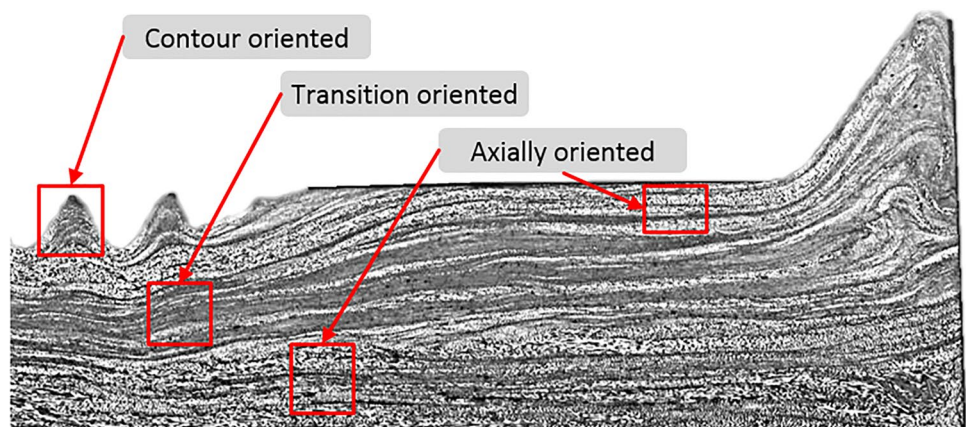


**Table 1** Input data to calculate the pre load of the joint

Fastener	$\mu_{K_B}$	$\psi_B$	$Q_B$	$d_{2B}$ (mm)	$d_{K_B}$ (mm)	$M_{VK}$ (N m)
3/16" Ti	0.31	3.3°	13.8°	4.4	8.1	10
3/16" CF-PEEK	0.3	3.3°	14.7°	4.4	8.1	2
1/4" CF-PEEK	0.3	2.9°	14.7°	5.7	10.2	4

**Table 2** Input data for joint spring models for the laminates

	$t_{L,LE}$	$b_{L,LE}$	$l_L$	$l_{LE}$	$d_H$
Geometry					
For 3/16" bolt	3 mm	30 mm	28.8 mm	33.8 mm	4.82 mm
For 1/4" bolt			38.1 mm	44.85 mm	6.37 mm
Homogenised laminate properties					
	$E_x$	$E_y$	$E_z$	$G_{xz}$	$\nu_{xy}$
	60.26 GPa	60.26 GPa	6.77 GPa	4.84 GPa	0.3

transition zone the fibre orientation is quasi three-dimensional. In the in groove of the thread an axially orientation of the fibres is visible. The thread consists of a helical fibre orientation, which results from the matrix flow process during production [36].

Each specimen is mounted with two fasteners. Torques vary with regard to the used fastener system (see Table 1). According to the data sheet the 3/16" Ti-fasteners are mounted with a torque of 10 N m. The fastening torque for the 3/16" and 1/4" CFRP-fasteners is set in consultation with manufacturing company icotec to values that no inter fibre damages occur during assemble of the specimens. Therefore 3/16" CF-PEEK-fasteners are all mounted with a torque of 2 N m and for the 1/4" CF-PEEK-fasteners 4 N m fastening torque is used. The different fastening torques for each fastener system lead to different pre loads for each specimen configuration. The coefficient of friction  $\mu_{K_B}$  in the contact areas between bolts and laminate and between the laminate plates are estimated for each fastener configuration based on values from similar joint configuration in the literature [37, 38].

Parameters for the laminate plates and the CF-PEEK-fasteners are obtained by mechanical tests and a calculation

with the software ELAMX2 (see Table 2). These test are performed in accordance to ASTM Standards for tensile loading [39] and compressive loading [40]. Based on simple compression and tension tests of the CF-PEEK-bolts, the young's modulus for the CF-PEEK Bolts is determined. For the countersunk head of the CF-PEEK-fasteners the young's modulus  $E_{BK}$  is estimated by 80% as a fitting factor of the modulus for the shaft (see Table 3). This assumption is made in this work to take the observed fibre structure within the area of the countersunk head (see Fig. 2) into account for the following calculations.

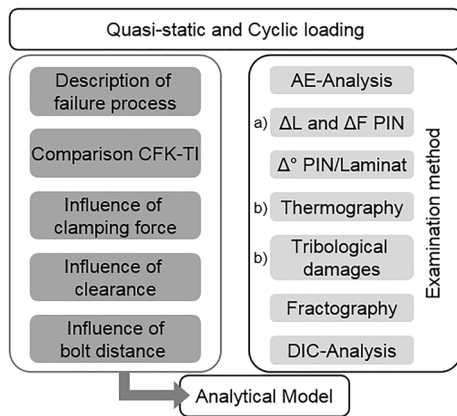
### 2.1.1 Testing procedure and measurement set-up

Figure 3 demonstrates the parameters and the corresponding methods of the test program for the investigation of the failure mechanisms of SLS-joint in quasi-static and cyclic loading. The test results are used, to fully describe these new type of CF-PEEK-fastener system in a SLS-joint by an enhanced analytical model. The focus in this paper is the description of the failure process for the CF-PEEK-fastener and set their performance in relation with the Titanium-fastener. Furthermore different examination methods, such as AE-Analysis and fractographic investigations techniques according to Greenhalgh [35] are used.

For the static tests, SLS-joints are loaded in a Zwick Roell 100 kN universal testing machine with a constant crosshead speed of 1.5 mm/min. The ultimate failure load is measured directly as the peak load. The fatigue loading tests for the three different specimen configurations are performed with the stress ratio  $R = \sigma_{min}/\sigma_{max} = 0.1$  using a 100 kN servo-hydraulic test machine (Instron GmbH). The test frequency was set at 5 Hz to prevent internal thermal heating, which might cause degradation effects by the friction between the two laminate plates. All experiments are performed at a room temperature of  $T = 23$  °C and ambient relative humidity of 50%. All test results are presented in

**Table 3** Input data for joint spring models for the three investigated fasteners

	3/16" Ti-fastener			3/16" CF-PEEK-fastener			1/4" CF-PEEK-fastener		
Geometry	$d_B$	$h_{BK}$	$\phi_B$	$d_B$	$h_{BK}$	$\phi_B$	$d_B$	$h_{BK}$	$\phi_B$
	4.8 mm	1.4 mm	100°	4.8 mm	1.4 mm	100°	6.35 mm	1.6 mm	100°
Parameter	$E_B$	$E_{BK}$	$\nu_B$	$E_B$	$E_{BK}$	$\nu_B$	$E_B$	$E_{BK}$	$\nu_B$
	110 GPa	110 GPa	0.3	44 GPa	32.2 GPa	0.3	44 GPa	32.2 GPa	0.3



**Fig. 3** Test program performed: Investigation on the failure mechanisms of CFRP Single-lap shear joint; **a** only in quasi-static load tests and **b** only in cyclic loading tests

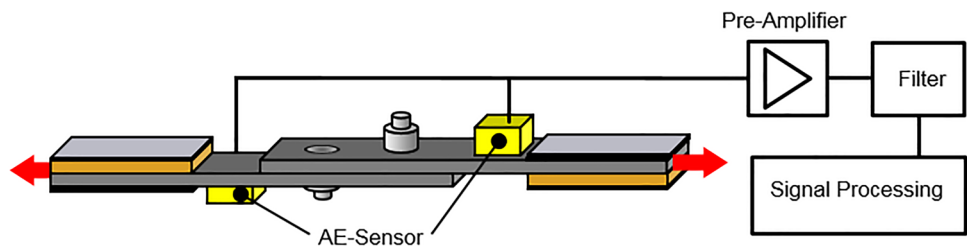
force–displacement curves or force over cycles diagrams. Force, displacement and the term stiffness have in this context not the meaning of a material property as the SLS-specimen represents a structural part.

### 2.2 Experimental instrumentation

For quasi-static tests the elongation of each specimen is measured with an inductive extensometer clamped to the specimen (Zwick Roell, Germany). In fatigue load tests, the alternation of length is measured with a contact free laser extensometer from Fiedler Optic, Germany. To detect the AE-signals a simple set-up is used, consisting of two wide-band differential (WD) AE sensors operating from 100 to 1.000 kHz, clipped to the specimen as displayed in Fig. 4. Detected AE-signal are amplified by 20 dB and process by a PCI-2 measuring board implemented in a Micro-II from the Mistras Group (Germany).

Consequently, tests are stopped at certain AE-events and inspections of the microstructure are analysed to characterize the distinct failure modes. As inspection methods for the failure modes of the joints ultrasonic C-scans, X-Ray and light microscopy on cut views are applied. To obtain the cut views for this purpose, in tension loaded specimens are prepared by polished cut images in the cross section in loading direction of the joint.

**Fig. 4** Test set-up: SLS-joint with two fasteners and mounted AE-sensors



## 3 Results and discussion

This chapter is divided into three main parts:

- Test results of quasi-static SLS tension tests for the three types of fastener systems and detailed discussion.
- Analytical model to calculate the system behaviour of an SLS-joint with CF-PEEK-fastener in the undamaged range of loading.
- The degradation process for the CF-PEEK-fastener under fatigue loading is described and discussed.

### 3.1 Failure process of SLS-joints under quasi-static loading

Representative force—displacement curves of the SLS tensile tests with either 3/16" Ti-fasteners, two 3/16" CF-PEEK-fasteners or 1/4" CF-PEEK-fasteners are shown in Fig. 5. From the overall behaviour it can be stated that the Ti-fasteners bear higher loads than the corresponding CF-PEEK-fasteners (3/16" size). Whereas the CF-PEEK-fasteners with 1/4" in diameter carry about the same max. load, resulting in a CF-PEEK-weight saving of 4% compared to the Ti-fastener.

In the load case in which all joint partners are in full contact, the slope of the force/displacement curves between 0.3 and 0.5 mm, indicate that the stiffness of specimens with CF-PEEK-fasteners is up to 30% lower than for specimens with Ti-fasteners.

#### 3.1.1 Description of failure process of SLS-joints using acoustic emission

Taking a more detailed look on the load–displacement behaviour of the joint up to a load of 6000 N (Fig. 6a), the changes in the stiffness of the joints can be correlated for each fastener configuration to the five stages of joint behaviour classified by Stocchi et al. [5]: no-slip, slip, full contact, damage and finale failure (see Fig. 6b). The experimental results differ from theory: Due to stick–slip effects in the joint, tolerances of the borehole and its position and fastener geometry the different stages are not as distinct as presented in the literature. However, the stages no-slip, slip and full contact can be dedicated in Fig. 6a.

**Fig. 5** Comparison of SLS-specimens with different fastener systems: either Ti-fasteners or CF-PEEK-fasteners in a load displacement diagram

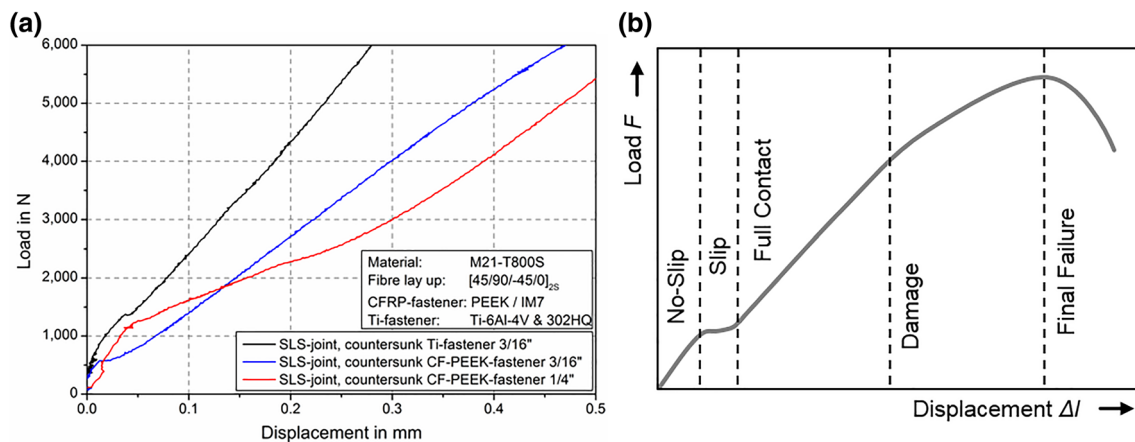
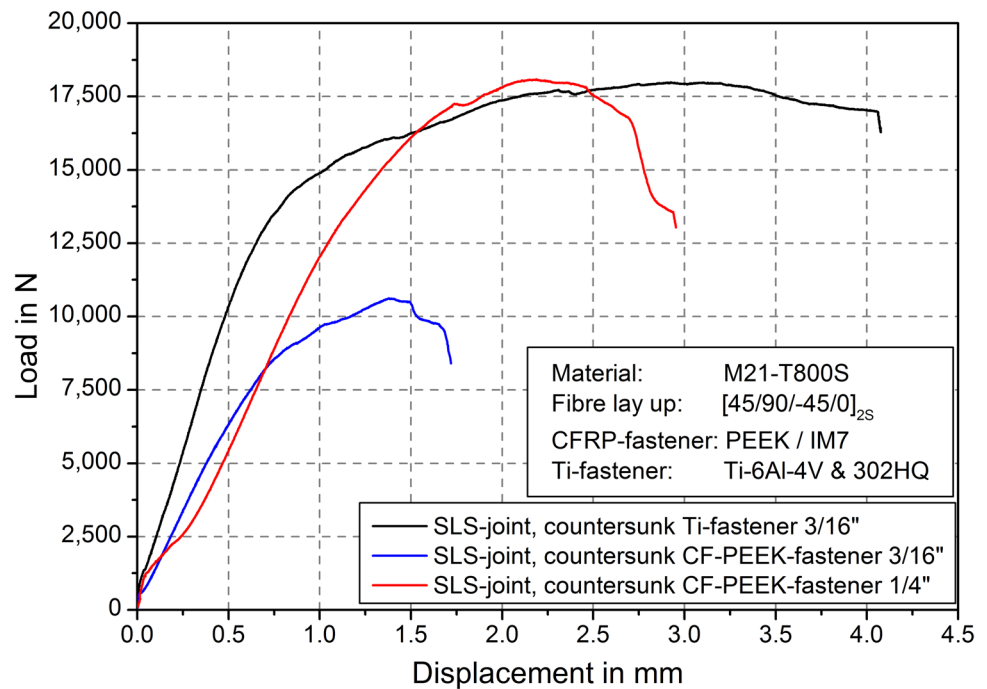


**Fig. 6** **a** Joint behaviour for loads below 6000 N, of SLS-joints with different fastener systems, comparison of Ti-fasteners with CF-PEEK-fasteners (section from Fig. 5). **b** Five stages classified in the

joint behaviour, the first three stages correspond weakly to the stages of the test results in the left figure [5]

In Fig. 6a the no-slip stage is the frictional connection and has the highest stiffness for all three fastener systems. Thus within this region the stiffness of the joint only depends on the stiffness of the laminate plates. The maximum of possible load transfer by the joint is correlated to the applied clamping force of the bolt and the coefficient of friction. Therefore, joints mounted with Ti-fasteners and torque of 6–10 Nm are capable to bear higher loads than the joints mounted with CF-PEEK fasteners and smaller mounting torques.

When the maximum load transferred by friction is exceeded, the plates start to slip by the amount of the clearance between the bolts and the holes. The slip stage for the three configurations depends on the geometric properties of the joint. The transition between the joint loading stages exhibits a smooth change in stiffness for all fastener configurations, as shown in Fig. 6a. Several effects affect this behaviour of the joint. As the laminate plates start to slip, a change from static to kinetic friction causes a change in the slope. Furthermore, different geometry properties of fasteners, holes and the distortions of primary and secondary

bending lead to an increasing contact area between the joint partners. Therefore, the transition between the stiffness of the slip stage and the full contact phase appears to increase smoothly. The stiffness of the fastener perpendicular to the load axis, has a high impact on the trend of the stiffness in the full contact stage. For the three configurations different stiffness trends are clearly visible resulting from the shear modulus of each fastener (see Table 3). The shear stiffness of a titanium fastener is higher than the shear stiffness of the CF-PEEK-fasteners. The two distinct stiffnesses of the joint with a 1/4" CF-PEEK-fasteners can be explained with the semi- and full-contact stage of the SLS-joint, introduced by Egan et al. [25].

In the full contact zone positive locking between the laminate plates and bolts transfers the load. Due to local non-uniform contact areas between the joint partners, the stiffness of a joint in full contact is lower than in the no-slip stage. In addition, specimens with Ti-fasteners exhibit a higher stiffness than specimens with CF-PEEK-fasteners. A possible explanation is the higher shear modulus of the Ti-fasteners versus the CF-PEEK-fasteners.

The next stage is characterised by a steady reduction in stiffness and first occurring damages. For CFRP-plates joined with Ti-fasteners, the loss in stiffness is very significant (compare Fig. 5). At the borehole edges, bearing damage is detected. Literature suggest that plastic deformation caused by shear in the bolt shank, where it is aligned to the faying surfaces, have to be taken into account in this stage [5].

The failure process of the CFRP-joints in the damage stage is slightly different. To get a more detailed information on the failure process AE-signals are recorded during loading of the three types of fasteners. To compare the system performance of the joints with 3/16" Ti-fastener, 3/16" CF-PEEK fasteners and 1/4" CF-PEEK-fastener exemplarily results of SLS-tests including the data of AE investigations are plotted (see Fig. 7a–c). The black line represents the load vs. displacement curve. During the entire tests AE-events (hits) are monitored. For the three different types of fasteners in the first three stages from no-slip til full-contact, the range of the peak frequency suggests, due to literature [26, 41], only matrix failure (80–200 kHz) and fibre matrix debonding (200–400 kHz) take place. Depending on the type of fastener at displacements of 0.6 mm for 3/16" Ti-fasteners, 0.4 mm for 3/16" CF-PEEK fasteners and 1.0 mm for 1/4" CF-PEEK fasteners, slight changes in stiffness are detected. Furthermore peak frequency of single hits reveal that first fibre failures (400–800 kHz) occurred in the joints. However, in the microscopic cut views, no damages in the laminate and CF-PEEK-fasteners can be found. This point defines the transition stage from the full contact stage to the damage stage in joint behaviour for all fasteners types (see Fig. 7a–c). Comparing the results for the joint

with 3/16" Ti-fasteners (see Fig. 7a) and CF-PEEK-fasteners (see Fig. 7b, c) reveal the differences in the damage development of the joints. The results of the SLS-tests show that a significant increase of accumulated energy, correlates with changes in stiffness of the joint. Therefore, an increase of the accumulated energy indicates a severe damage of the joint. In the SLS-Test with Ti-fastener (see Fig. 7a) a simultaneous increase of accumulated energy and hits indicates continuous damage propagation in the laminate [6, 42].

Load–displacement curves for joints with CF-PEEK fasteners including the results of the AE investigation show a different system behaviour (see Fig. 7b, c). First damages in bolts and laminates for the joints with 1/4" CF-PEEK fasteners can be detected at 85% of maximum load at 1.4 mm of displacement. At this point, an increase in the accumulated energy of the AE-signal is detected. Several types of damage can be observed in microscopic pictures of cut views from a SLS-specimen, at which loading is stopped after detecting first AE-signals with high-energy rates (see Fig. 8a, b). In the laminate plates, bearing damages are not detectable. Damages of the bolt and nut itself due to the mounting process can be excluded. Inter fibre fracture is detectable in the transient section between the countersunk head and bolt shaft (see Fig. 8a). Furthermore, inter fibre fracture is visible in the area of the first load carrying threads (see Fig. 8a). Cause of this failure mode is primary and secondary bending due to the load situation of the bolt in the laminate plates. Further loading leads a growth of single cracks and formation of new inter fibre failure, cracks in the matrix of the CF-PEEK fasteners as can be seen in Fig. 8b. This effect is also proven by the AE-signal characteristic in Fig. 7c, which excludes fibre fracture and the formation of large delaminations. At approximately 90% of maximum load, an increase of inter fibre fracture is observable and first bearing damage at the borehole can be found as well (see Fig. 8b). The position of the cracks depends on the fibre orientation in the CF-PEEK-fastener. Changes in fibre orientation, e.g., undulation along the bolt lead to a significant change in stiffness, which favours the initiation of cracks. This effect is visible in the thread region in Fig. 8b.

During the test series first failure occurrence is highly depended on the fibre orientation. It can be concluded that damages develop in areas with misoriented fibres, which has to be avoided during processing of CF-PEEK-fasteners.

The situation at finale failure of this joint is displayed in Fig. 9a. The main failure modes in the laminate plates are crushed fibres and delaminations. Also chip outs at the hole edges of the plates are visible (see Fig. 8b). Matrix failure and inter fibre failure are the dominant failure mode in the transition from head to shaft of the CF-PEEK-fastener (see Fig. 9c). Fibre fracture in the CF-PEEK-fastener is only detectable at the first pitch of the thread (see Fig. 9d). The different failure modes occur due to a combined load case

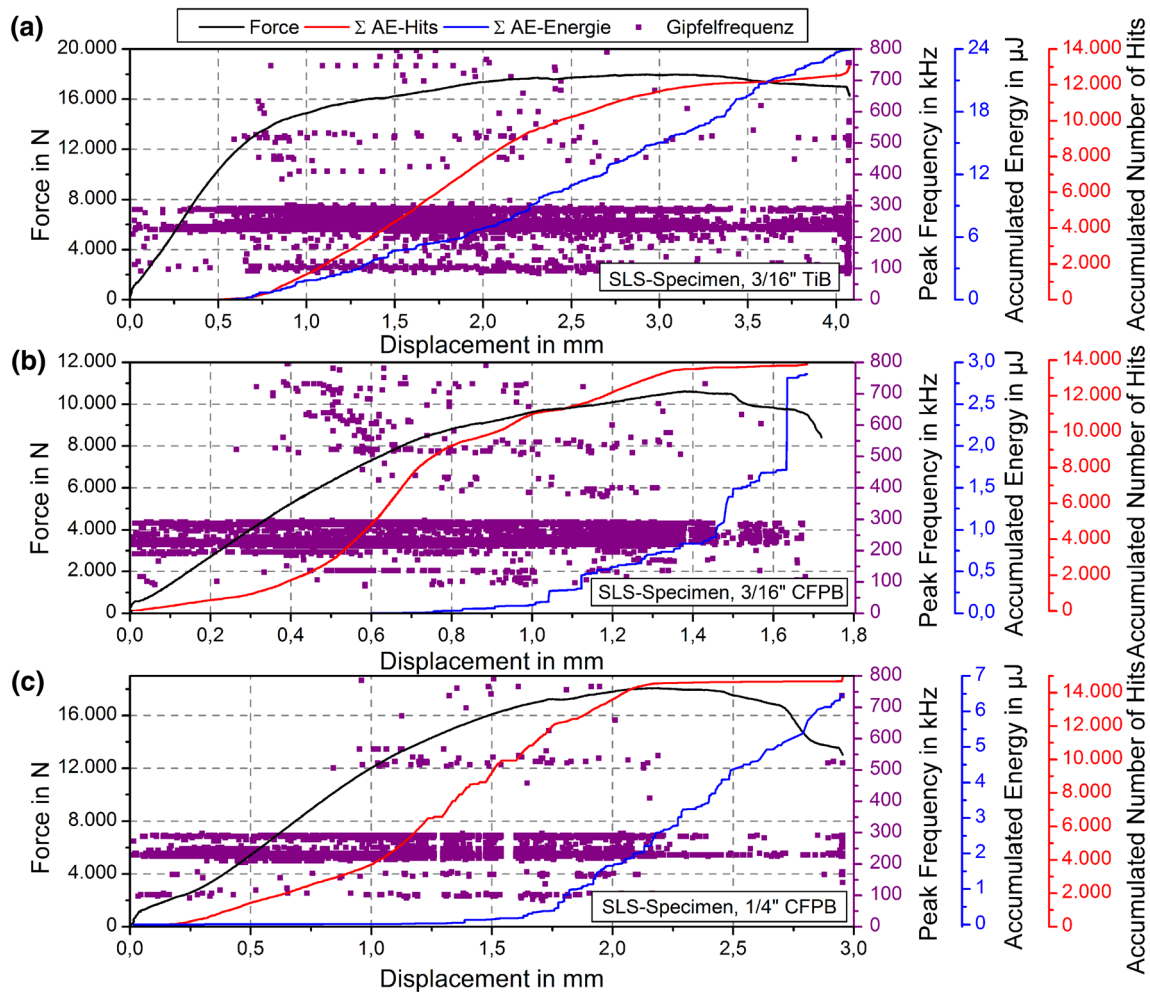


**Fig. 7** Load displacement curve with peak frequency for each hit, accumulated number of hits and accumulated energy of the AE-signals during representative tests of SLS-specimens each with two **a** 3/16" Ti-fastener, **b** 3/16" CF-PEEK-fastener and **c** 1/4" CF-PEEK-fastener

of shear and tension on the CF-PEEK-fastener. The shear forces on the bolt are introduced by the relative displacement of the laminate plates. Furthermore, the movement of the plates introduces a deflection onto the fastener. This primary bending of the fastener results in high stress in the first load carrying pitches of the thread. These stresses induce inter fibre failure and fibre failure shown in Fig. 9d. In progress of a SLS-test, the laminate starts to bend, this secondary bending of the specimen creates additional tension forces on the CF-PEEK-fastener head. The tension load on the countersunk head lead to a stress concentration in the transition from head to shaft.

After reaching the maximum load in the force displacement curve no change in the detected accumulated AE-hits is detected (compare Fig. 7c). Hence the accumulated AE-energy increases further. This phenomenon can be explained by continuously occurring damages which the AE-system detects as one failure. Furthermore, onwards from 2.3 mm displacement accumulated AE-energy escalates, which

corresponds to accumulated fibre failures (see Fig. 7c). In the nuts of the CF-PEEK—fasteners no failures are detectable for each single-lap shear test. Results for joints with 3/16" fastener exhibit the same characteristic signals in the failure process.

## 3.2 Analytical model describing the quasi-static behaviour of the SLS-Joints

### 3.2.1 Basic method

McCarthy et al. [4, 16]. introduced an spring mass model to describe the behaviour of bolted joints. A schematic of a single-lap joint with two CF-PEEK-fasteners together with the corresponding spring mass system is given in Fig. 10. The stiffness of the upper laminate is represented by  $K_{LE1}$  (i.e., spring stiffness between mass 4 and 5) and  $K_{L1}$ . The lower plate is described by  $K_{L2}$  and  $K_{LE2}$ .



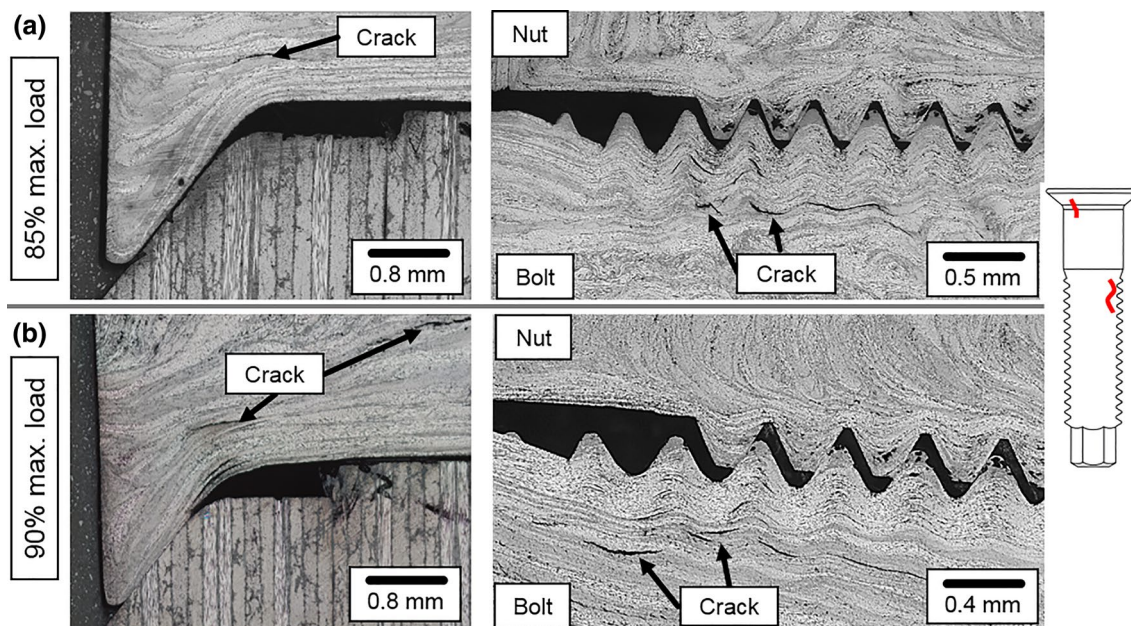


**Fig. 8** Optical microscopy cut view of failure mechanisms for 1/4" CF-PEEK-fastener configurations: **a** 85% max load inter fibre fracture shaft and thread; **b** 90% max load bearing damage in laminate and propagation of the inter fibre failure in shaft and thread region

The stiffness of the two CF-PEEK-fasteners are designated by the stiffness  $K_{B1}$  and  $K_{B2}$ . The joint is loaded with the force  $P$  at the mass 5. The behaviour of the spring mass model is based on the following basic assumptions [4]:

- Masses (1–5) only move in  $x$ -direction
- Springs have only a stiffness in  $x$ -direction
- Damages that might occur in the components of the joint are neglected for simplification
- Nonuniform bearing stresses are rated by the  $\beta$ -factor
- The orientation of the bolts is taken into account by the bolt stiffness and the  $\beta$ -factor
- Only static friction effects are implemented in the model
  - In the slip stage bolts and plates move frictionless
  - Stick slip effects are not included
- Both bolts exert the same clamping force
- The clearance is the same at both bolted joints
- Slip starts instantaneously and for the same value at each fastener.

### 3.2.2 Polynomial approach for the three loading stages of the joint

A polynomial approach is employed for the analytical model, allowing to describe the phases of the force displacement curve in Fig. 11 separately. The stiffness of each joint partner is used as a key factor for the analytical examination. The obtained functions of stiffness are merged into the spring mass

model to describe the loading situation of the joint. In the presented study, the analytical model maps the first three damage free stages in the linear-elastic region for a tension test of an SLS-specimen. The maximum applied force until no damage occurs in the joint is determined by the AE-results.

Tate and Rosenfeld [17] described the no-slip stage 1 (Fig. 11) by a linear force displacement trend; tension forces are only transferred by frictional forces. The maximum transferable friction force  $P_{slip}$  depends on the pre load  $F_{VK}$  and the coefficient of friction  $\mu$ . A higher pre load enables the joint to transfer more load. The pre load results from the mounting torque  $M_{VK}$  and the fastener properties: pitch angle  $\psi_B$ , angle of friction  $\varrho_B$ , effective friction-diameter  $d_{KB}$  of the nut and the effective pitch diameter  $d_{2B}$  (see 2). The mounting torque is given in Chap. 2.1 for the three fastener systems in this work.

$$P_{slip} = F_{VK} \times \mu \tag{1}$$

$$F_{VK} = \frac{2 \times M_{VK}}{d_{2B} \times \tan(\psi_B + \varrho_B) + d_{KB} \times \mu_{KB}} \tag{2}$$

The displacement of the SLS-specimen depends only on the laminate plates. The splice and end stiffness  $K_L$  for the laminate from Fig. 10 can be quantified using the expression 3, where  $E_{xL}$  represents the homogenised laminate modulus in the global  $x$ -direction,  $b_L$  the laminate width,  $l_L$  length of the laminate and  $t_L$  the thickness of the laminate.

$$K_L = \frac{E_{xL} \times b_L \times t_L}{l_L} \tag{3}$$

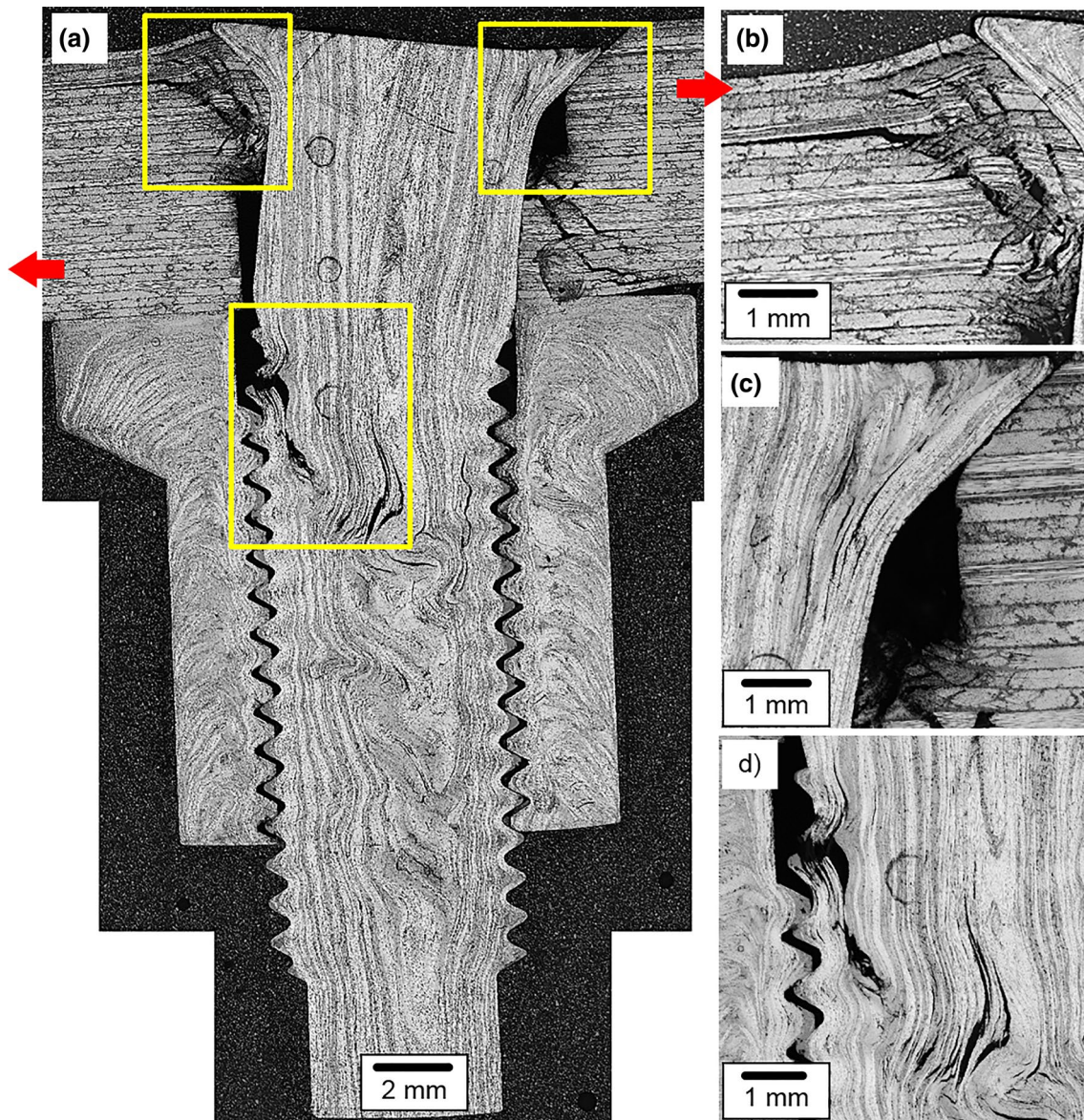


**Fig. 9** **a** Optical microscopy cut view of a finale failure of a CF-PEEK-fastener inside a SLS-joint, **b** failure modes in laminate plates, **c** failure modes in countersunk head of CF-PEEK-fastener, **d** failure modes in thread of CF-PEEK fastener

According to McCarthy et al. [16] a second term is needed to characterise the shear stiffness in the clamping area of the fastener. During loading of the joint, the strain generates a shear force, due to the fact, that countersunk head and nut are in contact with the laminate. Assuming the contact area of countersunk head and nut are equal, the transverse shear stiffens for each fastener is simply calculated by the contact area  $A_{BK}$  of countersunk head or nut, the shear modulus  $G_{xx_L}$  and the thickness of the laminate  $t_L$  (see 4).

$$K_{\text{shear}} = \frac{A_{BK} \cdot G_{xx_L}}{t_L} \quad (4)$$

The slip stage (see Fig. 10b) is calculated by the movement  $c$  of the laminate plates, according to the clearance between the shaft diameter  $d_B$  of the bolt and the bore hole diameter  $d_H$  (see 5).

$$c = d_H - d_B \quad (5)$$

The stiffness in the analytical approach for a bolted single-lap joint is very well described in the full-contact zone by Tate and Rosenfeld [17], Nelson et al. [18] and McCarthy et al. [16]. For the new designed CF-PEEK-fasteners, the analytical model is not sufficient, therefore, two extensions have been made. The original analytic model of Nelson et al. [18] for the stiffness of the joint is calculated using the expression (6).

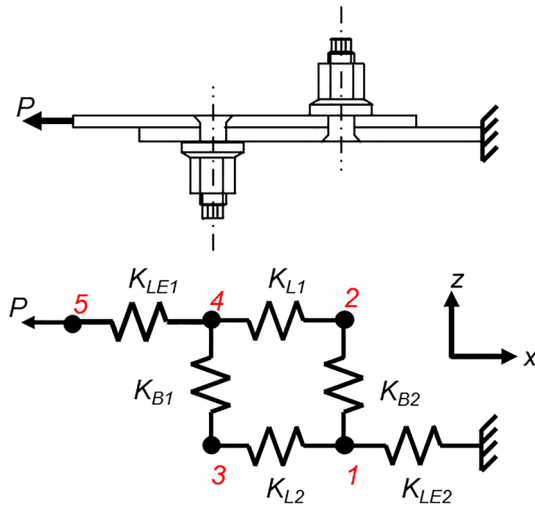


**Fig. 10** Two CF-PEEK-fastener, single-lap joint: illustration and corresponding spring mass model

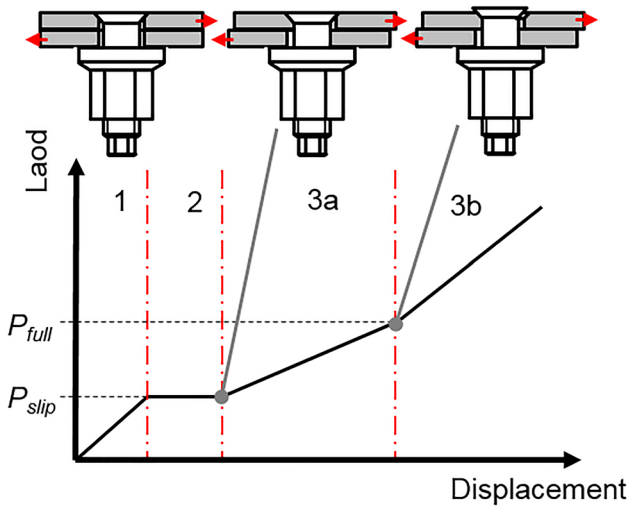


**Fig. 11** Load–displacement curve with three modelled stages of the joint behaviour; 1 no-slip stage, 2 slip stage, 3a semi-contact stage, 3b full contact stage

$$\frac{1}{K_{B1,full}} = \frac{2(t_{L1} + t_{L2})}{3G_{Bolt}A_{B1}} + \left[ \frac{2(t_{L1} + t_{L2})}{t_{L1}t_{L2}E_{B1}} + \frac{1}{t_{L1}(\sqrt{E_x E_y})_{L1}} + \frac{1}{t_{L2}(\sqrt{E_x E_y})_{L2}} \right] [1 + 3\beta] \tag{6}$$

In the equation the following variables are used:  $t_L$  laminate thickness,  $G_{Bolt}$  shear modulus of the bolt,  $A_B$  cross section of the bolt and  $E_x$  and  $E_y$  as the homogenised longitudinal and transvers modulus of the laminate. Nelson et al.

[18] introduce a term  $[1 + 3\beta]$  to the stiffness calculation of the bolt. Where  $\beta$  is the fraction of the bending moment on the bolt that is reacted by nonuniform bearing stresses across the thickness in a SLS-joint due to the eccentric loading. Therefore, it takes primary bending of the bolt and secondary bending of the laminate plates into account. The parameter  $\beta$  has to be chosen between 0 and 1. Choosing  $\beta$  as 1.0 represents a simple shear pin, to about 0.5 for a countersunk fastener, to small values for bolts with protruding heads becoming very small for the combination with of large washers with large diameter-to-thickness ratio.

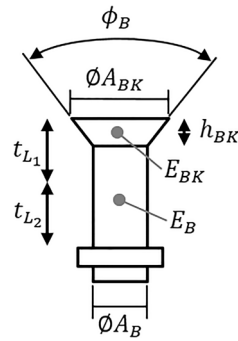
The anisotropic behaviour of the bolt was introduced into the model which uses isotropic material behaviour so far. The mayor adaption in the analytical model is due to the occurring failure mode in the countersunk head for the 3/16" and 1/4" CF-PEEK-fastener. Compared to the Ti-fastener, for the CRFP-fastener small plastic and elastic deformation are observed in the countersunk head during testing. To implement this anisotropic behaviour of the CF-PEEK-fastener, two differing moduli are introduced into the analytical model, one for the countersunk head and one for the shaft of the bolt (see Fig. 12).

The adaption of a stepwise form fit between the countersunk bolt with the borehole of the laminate was observed by Egan et al. [25] is the second adjustment of the analytical approach. Two stages are defined: the semi-contact stage and the full contact stage. In the semi-contact stage (see Fig. 11 number 3a) both, countersunk laminate and bolt slide as a unit, reducing the clearance between bolt and non-countersunk laminate. Once bolt-shaft and laminate are in contact, the next stage, the full contact stage (see Fig. 11 number 3b) is initiated. The countersunk laminate slides relatively to the bolt, until the cylindrical part of the laminate makes contact with the bolt shaft, and the clearances are closed. At this point, the joint becomes significantly stiffer.

The observed changes of contact areas are introduced into the approach of Nelson presented in Eq. 6 by adjusting the three terms for, the shear deformation of the bolt, the bearing deformation of the bolt and laminates. Furthermore the semi-contact stage and the full contact stage (see Fig. 11) have to be calculated separately.

The first Term of the bolt stiffness describes its shear deformation. In the semi-contact stage it is assumed that the force application point is in the centre of the lower laminate and in the bolt head centre in the upper laminate (see Fig. 11). The total deformation  $\Delta l_{shear,semi}$  of the bolt is the sum of the deformation of the bolt shaft  $\Delta l_B$  and the bolt head  $\Delta l_{BK}$ . As a result of the thrust load the deformation of the bolt can be calculated with the equations in (7) using the laminate thicknesses  $t_{L1}$  and  $t_{L2}$ , shear modulus of the bolt head  $G_{BK}$  and bolt shaft  $G_B$ , cross section of the bolt head  $A_B$  and bolt shaft  $A_B$  and the high of the bolt head  $h_{BK}$ :

**Fig. 12** Description of the CF-PEEK-fastener model for the analytical approach



$$\Delta l_{\text{shear,semi}} = \Delta l_B + \Delta l_{BK} = \frac{\tau \times h}{G_B} + \frac{\tau \times h}{G_{BK}} = \left[ \frac{2(t_{L1} + t_{L2})}{3G_{B1}A_{B1}} + \frac{2t_{L1} - 4h_{BK1}}{3G_{B1}A_{B1}} + \frac{4h_{BK1}}{3G_{BK1}(A_{BK1} + A_{B1})} \right] \times P \quad (7)$$

In the full contact stage it is assumed that the force application point is in the centre of the upper and lower laminate and the influence of the bolt head is vanishingly small. The deformation of the bolt results as before from the thrust load and is calculated as:

$$\Delta l_{\text{shear,full}} = \frac{\tau \times h}{G_B} = \left[ \frac{2(t_{L1} + t_{L2})}{3G_{B1}A_{B1}} \right] \quad (8)$$

The second term of the bolt stiffness presents the bearing of the bolt. The equations for semi-contact stage (9) and full contact stage (10) represent a displacement of the bolt due to the surface pressure between bolts and bore wall. The acting stress is a quotient between the attacking force  $P$  and the perpendicular projected support surface. To take the relation of the elastic modulus of the bolt head and bolt shank into account, both material parameters are weighted by their heights.

$$\Delta l_{N,\text{semi}} = 2 \times [\Delta l_{N,1} + \Delta l_{N,2}] = \left[ \frac{2}{h_{BK1}E_{BK1}} + \frac{2}{t_{L2}E_{B1}} \right] \times P \quad (9)$$

$$\Delta l_{N,\text{full}} = 2 \times [\Delta l_{N,1} + \Delta l_{N,2}] = \left[ \frac{2(t_{L1} + t_{L2})}{t_{L1}t_{L2}E_{B1}} + \frac{2h_{BK1}(E_{B1} - E_{BK1})}{t_{L1}E_{B1}(t_{L1}E_{BK1} - h_{BK1}E_{B1} + h_{BK1}E_{BK1})} \right] \times P \quad (10)$$

The third term of the bolt stiffness presents the bearing deformation of the laminates. Semi—and full contact stage differ only in the bearing surface of the bolt on the bore wall. Further changes are not necessary in relation to the

approach from Nelson et al. [18] for determining the bearing deformation.

$$\Delta l_{N,\text{semi}} = \left[ \frac{1}{h_{BK1}(\sqrt{E_x E_y})_{L1}} + \frac{1}{t_{L2}(\sqrt{E_x E_y})_{L2}} \right] \times P \quad (11)$$

$$\Delta l_{N,\text{full}} = \left[ \frac{1}{t_{L1}(\sqrt{E_x E_y})_{L1}} + \frac{1}{t_{L2}(\sqrt{E_x E_y})_{L2}} \right] \times P \quad (12)$$

The bolt stiffness for the two stages with an anisotropic CF-PEEK-fastener is now calculated for the semi-contact stage as presented in Eq. (13) using Eqs. (7), (9) and (11) whereas the full contact stage as shown in Eq. (14) is calculated using the Eqs. (8), (10) and (12).

$$\frac{1}{K_{B1,\text{semi}}} = \frac{2(t_{L1} + t_{L2})}{3G_{B1}A_{B1}} + \frac{2t_{L1} - 4h_{BK1}}{3G_{B1}A_{B1}} + \frac{4h_{BK1}}{3G_{BK1}(A_{BK1} + A_{B1})} + \left[ \frac{2}{h_{BK1}E_{BK1}} + \frac{2}{t_{L2}E_{B1}} + \frac{1}{h_{BK1}(\sqrt{E_x E_y})_{L1}} + \frac{1}{t_{L2}(\sqrt{E_x E_y})_{L2}} \right] [1 + 3\beta] \quad (13)$$

$$\frac{1}{K_{B1,\text{full}}} = \frac{2(t_{L1} + t_{L2})}{3G_{B1}A_{B1}} + \left[ \frac{2(t_{L1} + t_{L2})}{t_{L1}t_{L2}E_{B1}} + \frac{2h_{BK1}(E_{B1} - E_{BK1})}{t_{L1}E_{B1}(t_{L1}E_{BK1} - h_{BK1}E_{B1} + h_{BK1}E_{BK1})} + \frac{1}{t_{L1}(\sqrt{E_x E_y})_{L1}} + \frac{1}{t_{L2}(\sqrt{E_x E_y})_{L2}} \right] [1 + 3\beta] \quad (14)$$

The following variables are used in the equations:  $t_L$  as laminate thickness,  $G_B$  shear modulus of the bolt,  $A_B$  cross section of the bolt,  $E_{BK}$  young's modulus of the bolt head and  $E_B$  young's modulus of the shaft (compare Fig. 11). The terms in the first row from  $K_{B1,\text{semi}}$  and  $K_{B1,\text{full}}$  describe their shear deformation. Terms in the second row apply the bearing deformation of the bolt, respectively the countersunk head. The third row of the stiffness calculation quantifies the bearing deformation of the laminates with  $E_x$  and  $E_y$  as the homogenised longitudinal and transvers modulus of the laminate. The term  $[1 + 3\beta]$  adjusted by Nelson et al. [18] to the bolt stiffness calculation is also assumed. As in this work countersunk fasteners are used,  $\beta$  is also set to 0.5 for countersunk fasteners as  $\beta$  is understood more as a geometric factor.

The transition from the semi to the full contact stage is marked by reaching the transition force  $P_{full}$ . By reaching this force the elongation of the bolt in longitudinal direction is sufficient that the gap between the upper bolt shank and the laminate is closed and the laminate is complete contact with the bolt. Furthermore the full contact is dependent on the geometric constrain of the displacement  $c$ , die elongation  $\Delta l$  of the bolt and die countersunk angle  $\phi_B$  (see Eq. 15)

$$\Delta l = \frac{\frac{1}{2} \times c}{\tan \frac{\phi_B}{2}} \tag{15}$$

It is assumed that the bolt is loaded with the total tensile force  $P_{full}$  in its longitudinal direction. The implied strains in the bolt shaft and bolt head must be considered with their assigned moduli. To simplify the force application situation, it is assumed that force acts in the centre of the laminate and at one-third of the bold head height. The deformation of the bolt then can be calculated as:

$$\Delta l = P \times (\Delta l_B + \Delta l_{BK}) = P \times \left[ \frac{t_{L1} + h_{BK} + \frac{1}{2}t_{L2}}{E_B A_B} + \frac{0.3h_{BK}}{E_{BK} [0, 3(A_{BK} - A_B) + A_B]} \right] \tag{16}$$

The transition from semi-contact to full contact is marked by reaching the transition force  $P_{full}$  which is calculated as the combination of Eqs. (15) and (16) as follows:

$$P_{full} = c \times \left[ 2 \tan \frac{\phi}{2} \left( \frac{t_{L1} + h_{BK} + \frac{1}{2}t_{L2}}{E_B A_B} + \frac{h_{BK}}{E_{BK} [(A_{BK} - A_B) + \frac{1}{0.3}A_B]} \right) \right]^{-1} \tag{17}$$

Influencing geometric factors are the thickness of the laminate  $t_L$ , the height of the countersunk head  $h_{BK}$ , cross section of the bolt  $A_B$ , the bearing area of the countersunk head  $A_{BK}$  and the countersunk head angle  $\phi$ . Young’s modulus of the bolt shaft  $E_B$  and the bolt head  $E_{BK}$  define the stress–strain characteristic of the bolt.

### 3.2.3 Analytical modelling

The spring mass model enables to describe each mass with an equation of motion using the free-body diagram.

Figure 13 illustrates the free-body diagram for mass 4 at half-contact of the bolt.

The equation of motion can be written as:

$$m\ddot{x}_4 - K_{L1}x_2 - K_{B1}x_3 + (K_{LE1} + K_{L1} + K_{B1})x_4 - K_{LE1}x_5 = K_{B1}(c_1 - u_1) + P_{slip1}, \tag{18}$$

where  $x_i$  is the displacement in  $x$ -direction for the mass  $i$  ( $i=2, 3, 4, 5$ ),  $c_1$  represents the overall displacement at bolt 1,  $u_1$  is the maximum displacement of the bolt and  $\ddot{x}_4$  is the acceleration of mass 4. For quasi-static loading, the acceleration is set to zero and is, therefore neglected, leading to the linear equation system of (19). The solution of the equations is computed with MATLAB Simulink.

$$[K]\{x\} = \{F\} \tag{19}$$

The linear equation system is solved for each stage with the stiffness terms from Chap. 3.2.2 which are introduced into the matrix  $[K]$  in (20) and the corresponding force vector from (21). In all stages the stiffness of the laminate  $K_L$  and  $K_{LE}$  are used,  $i$  is set for each calculated stage as followed:

- In no-slip stage in the stiffness matrix  $[K]$  (20)  $K_i$  represents the laminate shear coefficient  $K_{shear}$ . The load vector is chosen on the assumption that no relative movement of the laminates is detectable. The no-slip stage lasts until the load vector exceeds the static friction force and the laminate starts to slip at  $P_{slip}$ .
- The half contact stage is modelled with the bolt stiffness  $K_{B,semi}$ . The transition from the half to the full contact stage is marked by the force  $P_{full}$ , where  $u$  is the deformation factor and  $c$  the movement according to the clearance.
- The full contact stage is defined by the bolt stiffness  $K_{B,full}$ , where  $v$  displays the deformation factor. The maximum force  $P_{max}$  defines the end of the full contact stage.

Based on the assumptions of the analytical model the maximum load is limited to the linear-elastic behaviour and no plastic deformation is allowed to occur in the simulation of the quasi-static SLS-test.

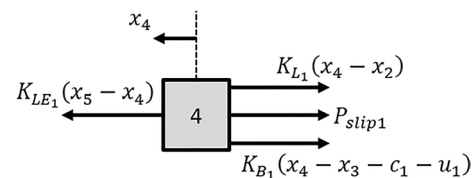


Fig. 13 Free-body diagram for mass point 4 in half-contact

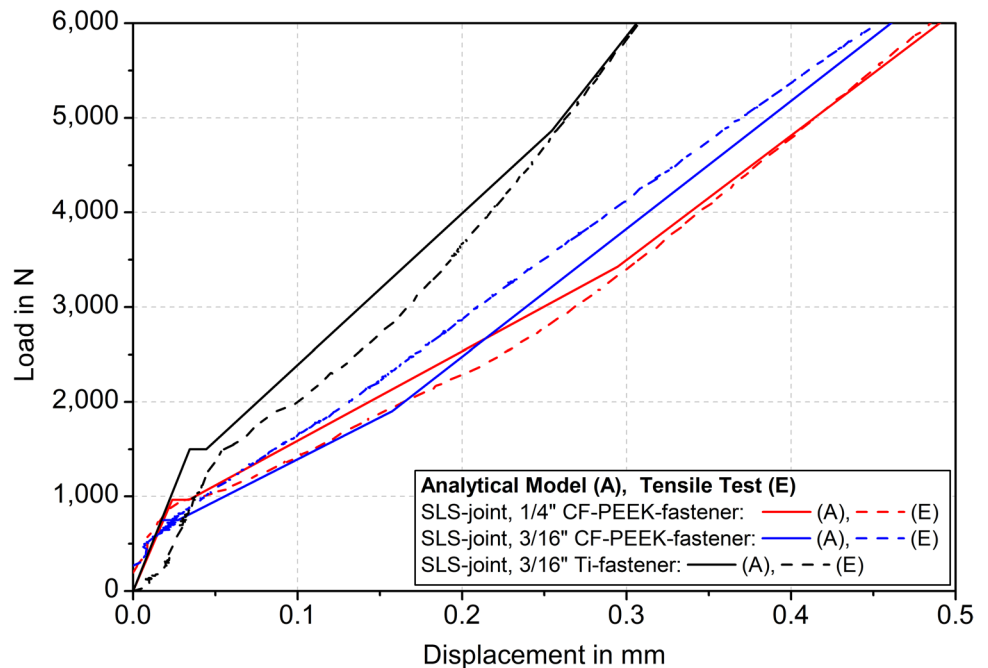
$$[K] = \begin{bmatrix} \begin{pmatrix} K_{LE_2} \\ +K_{L_2} \\ +K_{i_2} \end{pmatrix} & -K_{B_{2i}} & -K_{L_2} & 0 & 0 \\ -K_{B_{2i}} & \begin{pmatrix} K_{L_1} \\ +K_{i_2} \end{pmatrix} & 0 & -K_{L_1} & 0 \\ -K_{L_2} & 0 & \begin{pmatrix} K_{L_2} \\ +K_{i_1} \end{pmatrix} & -K_{B_{1i}} & 0 \\ 0 & -K_{L_1} & -K_{B_{1i}} & \begin{pmatrix} K_{LE_1} \\ +K_{L_1} \\ +K_{i_1} \end{pmatrix} & -K_{LE_1} \\ 0 & 0 & 0 & -K_{LE_1} & K_{LE_1} \end{bmatrix} \quad (20)$$

3.2.4 Model validation by experimental results

The data for the spring mass model are taken from Tables 2 and 3. The parameter  $\beta=0.5$  is taken in this work as a suitable value for countersunk fasteners. In Fig. 14 the results of the analytical model are illustrated with representative test results for the three different fastener configurations in a force displacement curve. Generally, the model represents the test results in the undamaged region very well. As demonstrated in Fig. 6, the transition from the no-slip via slip stage to the contact stage are in the tests not as distinctive as in the model. The stiffness of the SLS-specimens during the frictional connection, which is characterized by the laminate stiffness, is comparable in the model and the tests. A pure slip cannot be detected in the tests. The behaviour of the joint in the transition from the first to the third stage

Force vector {F} for each stage			
No-slip	Half-contact	Full-contact	
$\begin{bmatrix} 0 \\ 0 \\ 0 \\ 0 \\ P_{slip} \end{bmatrix}$	$\begin{bmatrix} -K_{B_{2semi}} \times c_2 + u_2 + P_{slip_2} \\ K_{B_{2semi}} \times c_2 + u_2 - P_{slip_2} \\ -K_{B_{1semi}} \times c_1 + u_1 + P_{slip_1} \\ K_{B_{1semi}} \times c_1 + u_1 - P_{slip_1} \\ P_{voll} \end{bmatrix}$	$\begin{bmatrix} -K_{B_{2full}} \times v_2 + P_{full_2} \\ K_{B_{2full}} \times v_2 - P_{full_2} \\ -K_{B_{1full}} \times v_1 + P_{full_1} \\ K_{B_{1full}} \times v_1 - P_{full_1} \\ P_{max} \end{bmatrix}$	(21)

Fig. 14 Spring Mass Model for single-lap shear tests with either two 3/16" Ti-fasteners, two 3/16" CF-PEEK-fasteners or two 1/4" CF-PEEK-fasteners compared to representative quasi-static SLS tensile test, A analytical model, E experimental results



is a superimposition of the individual phases, because slide friction, stick slip effects and fabrication tolerances are not implemented in the model. However, the model matches the transition from no-slip to slip and semi-contact stage. In the semi- and full contact stage, the stiffness of the SLS-specimens with titanium fasteners is higher due to the high shear modulus of titan than the stiffness of the joints with CF-PEEK-fasteners.

The analytical model represents quite well the measured stiffness increase with the two stages (semi- and full contact) for all bolt configurations. A relevance ranking study is made of each parameter in the analytical model in correspondence to the joint stiffness with two 1/4" CF-PEEK-fasteners, for the no-slip, semi-contact and full-contact stage (see Fig. 15). The slip stage is only affected by the amount of clearance. Each parameter is variated systematically by ± 10% to determine their relevance. Due to the set-up of the analytical model, clearance, bolt diameter and borehole diameter should have a significant impact on the model results. Input parameters like clamping, force, clearance, bolt diameter, and borehole diameter only change the transition point between two stages and have no direct influence on the stiffness.

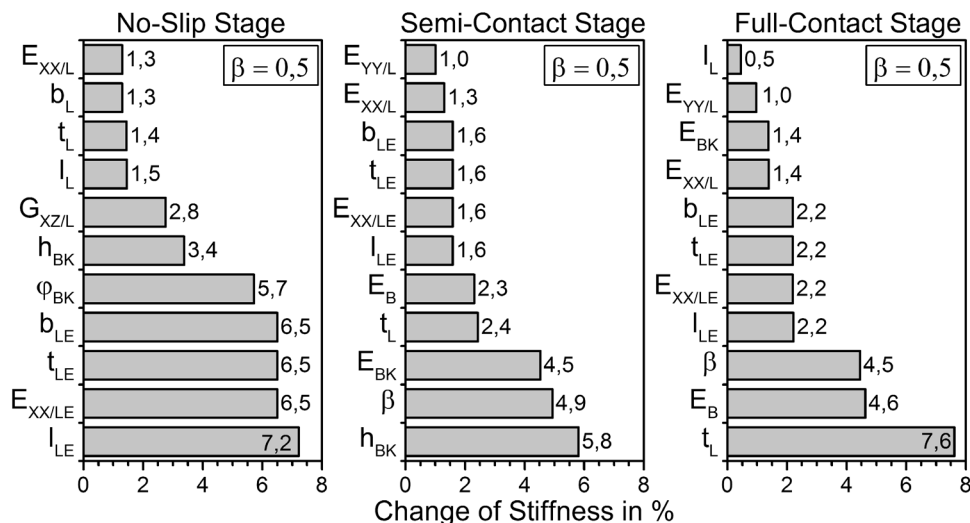
The no-slip stage is significantly influenced by geometric parameters such as specimen width  $b_{L/LE}$ , length properties of the specimen  $l_{L/LE}$  and the thickness of the laminate  $t_{L/LE}$ , (see Fig. 1). But also the material properties  $E_{X,L/LE}$  of the laminate plates set the stiffness of the joint. The smaller influence from the middle section of the specimen between the boreholes (index  $L$ ) compared to the laminate end (index  $LE$ ) on the joint stiffness, can be explained by the comparatively small initial length and the reciprocal proportionality of the laminate thickness  $t_L$  versus the shear stiffness  $K_{shear}$ . The shear stiffness (see 4) is calculated in this study by the projected bearing surface of the countersunk bolt using the

height of the bolt head  $h_{BK}$  and its angle  $\phi_B$ . As a result the dimensions of the bolt head take influence on the stiffness of the joint.

The results of the study for the semi-contact and full-contact stage reveal that due to contact between the fastener and the laminate, material properties of the CF-PEEK-fastener have a strong influences on the stiffness of joint, and therefore, on its behaviour. In the semi-contact-stage the fasteners are carrying a significant part of the applied load on to the joint. Therefore, the young's modulus of the bolthead and its height dominate the joint's stiffness. The material properties of the bolt-shaft and the thickness of the laminate dominate the joint stiffness in the full-contact stage, were the load is completely transferred by the fastener. Furthermore, the load-fraction-parameter  $\beta$  affects the system response significantly in the semi- and full contact stage [18]. This is expected, because the load-fraction-parameter represents the off axis loading of the joint into the calculation and is a key factor to the model.

Tolerances of the SLS-specimens, due to manufacturing processes and variation of material properties, lead to a scatter in results of the SLS-tests (see Chap. 3.1). To represent an expectancy range of the analytical approach in relation to the test results, a calculation with varying input parameters by ± 5% is carried out. The obtained range mapping of the absolute maximum and minimum for the chosen parameter variation is displayed in Fig. 16 for an SLS-joint with 1/4" CF-PEEK-fasteners: In the load-displacement diagram, the analytical model for joint parameters from Tables 2 and 3 are compared to three representative SLS-tests. The test results are within the expectancy range of the model marked with the black lines. The no-slip and the slip stage, which reach up to a displacement of 0.04 mm, do not fit completely (see enlargement Fig. 16).

Fig. 15 Percental influence of input parameters for a variation of ± 10% on the stiffness of the system for the no-slip, semi-contact and full-contact stage



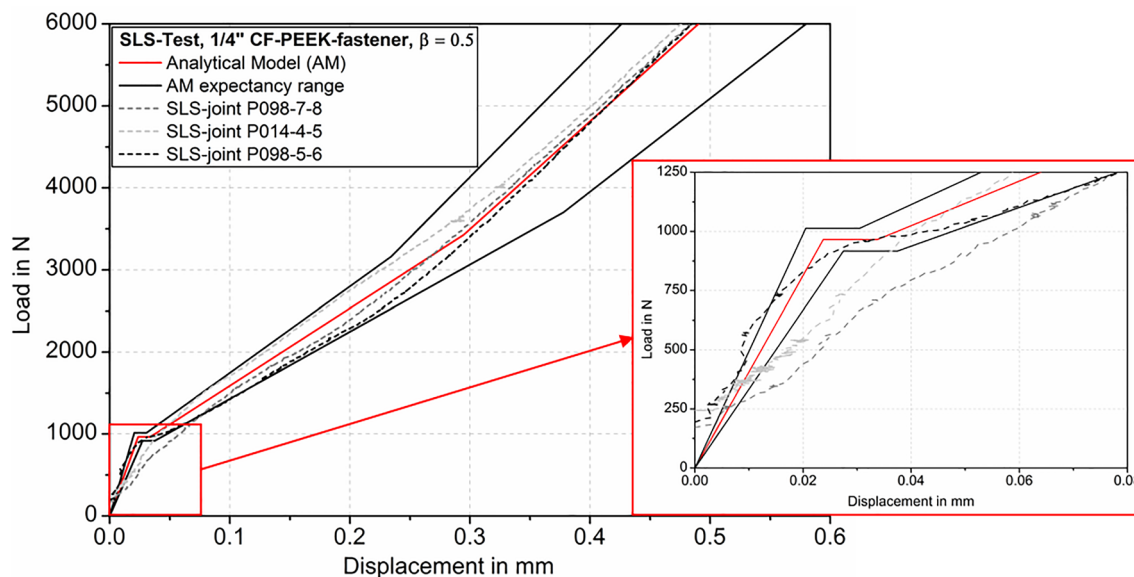


**Fig. 16** Load–displacement curves plotting the expectancy range of the analytical model versus test results of SLS-test for specimens with two  $\frac{1}{4}$ " CF-PEEK-fastener, including enlargement of the no-slip and slip stage

Reason for this is the idealized segmentation into the different stages by the analytical approach.

Starting from 0.1 mm displacement the expectancy range of the model fits the series of curves from the test nearly ideal. It can be concluded, that especially in the semi- and full-contact stage, the analytical model describes the trend of the test results very precisely. An estimation of joint behaviour for design purposes is, therefore, technically feasible.

### 3.3 Failure process of SLS-joint with CF-PEEK-fastener in fatigue loading

#### 3.3.1 Fatigue properties and life time

Bolted joints with the different fastener configurations are tested at different load levels in fatigue loading. The load levels are determined from the previously conducted quasi-static tensile tests. The results are plotted in a fatigue life diagram. At least 10 specimens of each configuration are tested in cyclic loading (see Chap. 2.1). The fatigue test results are presented in Fig. 17 including the quasi-static tensile strength with the corresponding mean deviation for each SLS-specimen configuration.

The partial regression lines in the diagrams are obtained by a linear fit of the logarithmic displayed fatigue data. The load level for the same fatigue life of the SLS-specimens with Ti-fasteners is higher than for specimens with CF-PEEK-fastener. Specimens with the small  $\frac{3}{16}$ " CF-PEEK-fasteners have the lowest fatigue resistance. In all cyclic tests with SLS-joints, the observed final failure mode is a fracture of the fasteners. Whereas, a bolt losing due to a

untightening of the nut could not be observed for any tested joint. The fatigue resistance of the three different specimen sets can be explained by the different material properties of each fastener-system. Especially the high shear strength of the titanium bolt results in higher load carrying capability of the joint. Disappointing is that the fatigue resistance of the CF-PEEK-fasteners is only between 60 and 55% of the static tensile load, whereas for the Ti-fastener cyclic loads from 85 to 75% are possible. The accelerated fatigue failure of the CF-PEEK-fasteners compared to Ti-fasteners, can be referred to damages such as inter fibre fractures, occurring at lower load levels as in the static failure process, and therefore, lead to inter fibre fractures, which develop in areas with a high stress concentration due to the loading conditions of the bolt. An accelerated degradation process due to heat dissipation, induced by friction between the laminate plates of the joint and internal friction due to shear forces in the fastener during cyclic loading, is possible. Pilot experiments launched with different loading frequencies at 1 Hz, 3 Hz and 5 Hz showed marginal effect in specimens' response. Thus, to eliminate heat dissipation, fatigue experiments with lower frequencies should be conducted. Nevertheless, for the current study such effects are neglected, considering low impact in the overall response.

For comparison of the potential of the new CF-PEEK fastener system with the conventional Ti-based system, it is suitable to normalize the properties by the weight of the bolts of each fastener and make the properties specific. The nuts are not taken into account in this calculation, given that a weight optimisation has to be executed.



**Fig. 17** Fatigue life results: maximum load versus number of cycles to failure

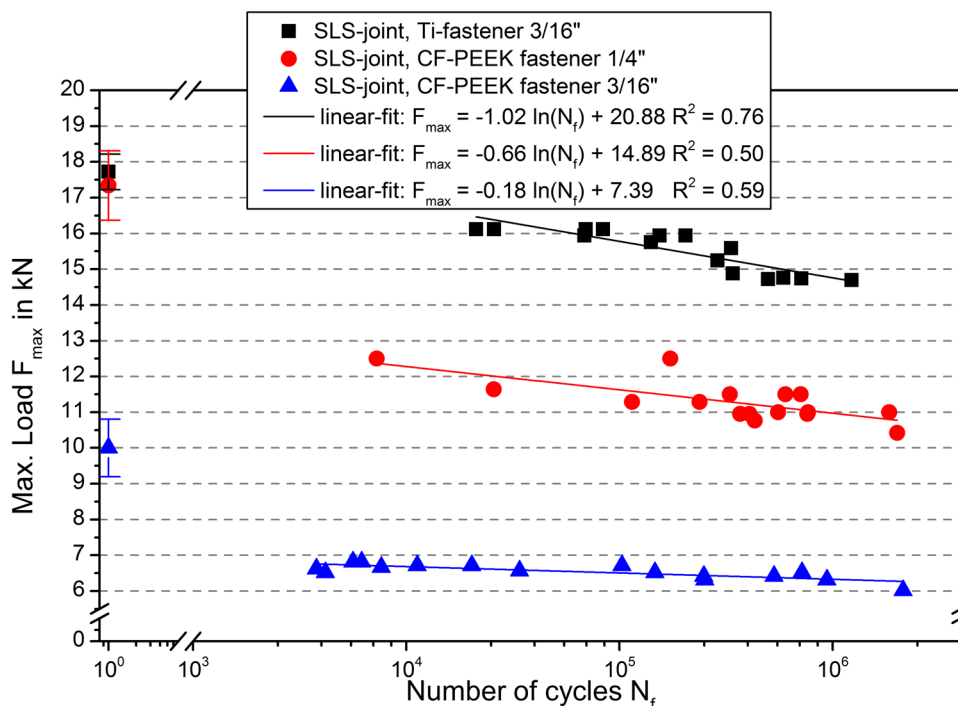
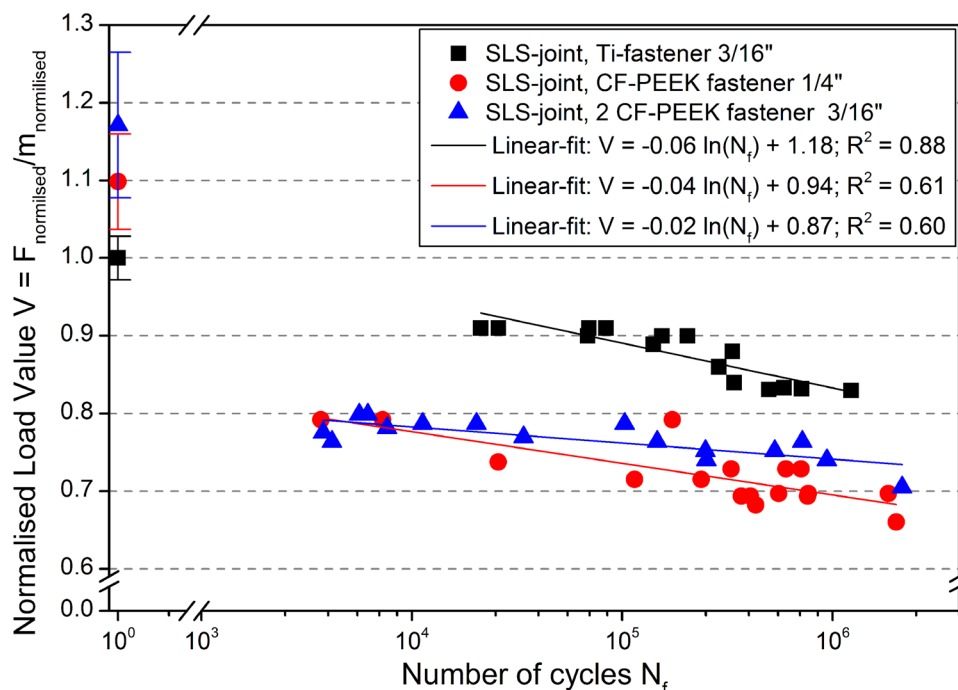


**Fig. 18** Fatigue life results: normalised load value versus number of cycles to failure



In Fig. 18 the data are normalised to the maximum tensile strength of the SLS-specimens with two Ti-fasteners and the corresponding weight of the Ti-bolts. Taking the weight of the bolts into account, the advantage of the CF-PEEK-fastener is obvious for the static loading. With a 1/4" CF-PEEK-fastener, a weight reduction for the fastener by 4%

is achieved, this increases the normalised tensile strength by approximately 10% and the normalised fatigue resistance is in the same range as the SLS-specimens with Ti-fasteners. For 3/16" CF-PEEK-fasteners, which have half the weight of Ti-fasteners, an increase of 18% for the maximum tensile load is detectable, however, the fatigue resistance decreases

by 10%. Early approaching inter fibre fractures in the countersunk head of the CF-PEEK-fasteners decrease the fatigue life performance. A redesign of the countersunk head and of the fibre orientation in the bolt could improve the load carrying capability of the CF-PEEK-fasteners significantly.

### 3.3.2 Failure process of the CF-PEEK-fasteners in fatigue loading

Due to the unexpected decrease in fatigue resistance of the CFRP fasteners in relation to their static tensile load and the Ti-fasteners, a closer look on the degradation of the CFRP fasteners is necessary. During fatigue loading the reduction in stiffness is often used to monitor damage development. Its change can be related directly to stress redistributions, which are expected to occur because of damages in joint partners. In general, the stiffness variation versus fatigue life curve is divided into 3 stages [43]. The description of the degradation and damage during fatigue life of the joints can be supported by monitoring the acoustic events. A detailed and representative investigation on the failure process for SLS-joints with  $\frac{1}{4}$ " CF-PEEK under cyclic loading is displayed in Fig. 19. Like in the quasi-static tensile tests, indication on damages can be extracted using the peak frequency of each AE-event, the accumulated number of hits and the accumulated energy. Using, the analysis of the AE-results in

combination with the stiffness reduction, damage effects can be evaluated in detail. Three distinctive stages are visible. In the first 4000 cycles, an increase in stiffness of the joint is detectable, accompanied by only a small acoustic activity. Interestingly, already 5% of the energy are emerged by these few AE-events. The detected peak frequencies of the signals in this section are between 100 and 300 kHz indicating matrix and inter fibre failure. Further investigations of the specimens with ultrasonic C-scans, and cut views reveal no significant damages of the joint. The increase in stiffness at the very first load cycles of the test are most probably setting effects of the fasteners in the joint. Due to small plastic deformation of the CF-PEEK fasteners, the shank is fitted well into the borehole, which leads to a larger load carrying surface.

The 2nd stage of the fatigue life is characterised by a rapid decrease of the stiffness (Fig. 19) caused by damages in the joint. AE-events with peak frequencies in the range of 0–300 kHz indicate fibre matrix debonding. Whereas the range between 400 and 800 kHz is resulting from fibre fracture. Cut views from specimens after 4% fatigue life, which corresponds to 3600 load cycles (Fig. 19) show first cracks in the matrix in the transition from head to shaft and small delaminations in the region of the first load carrying thread. With increasing number of load cycles the primary bending of the bolt and secondary bending of the SLS-specimen

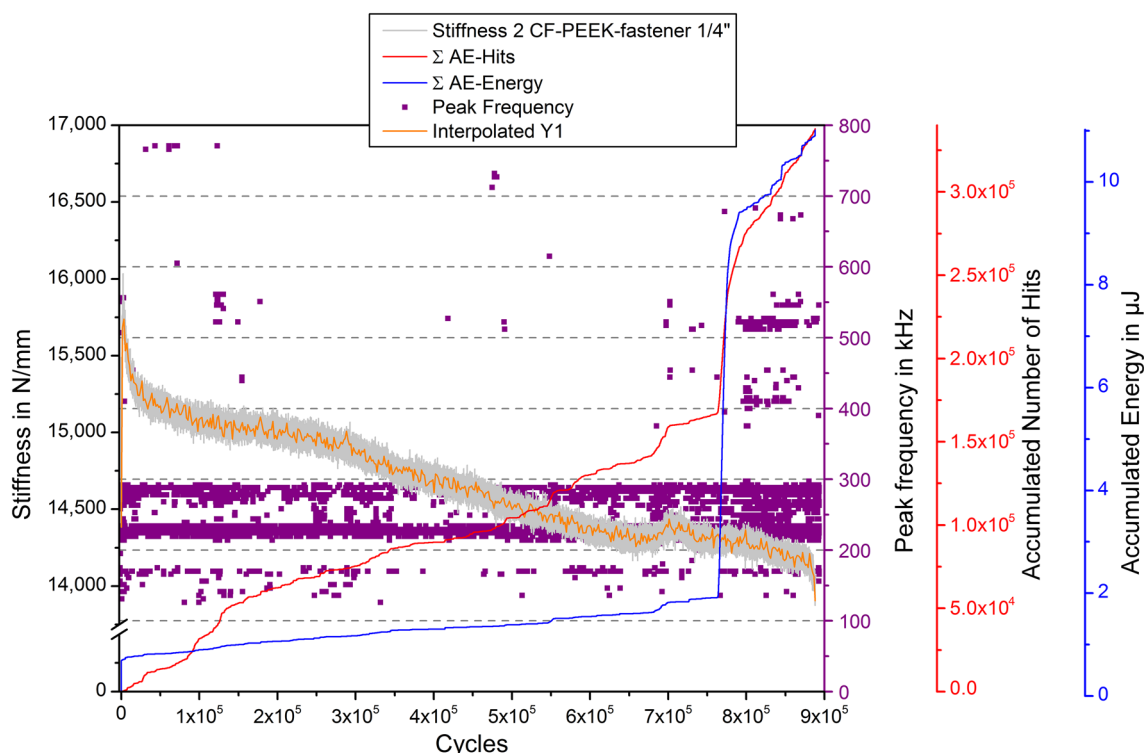


**Fig. 19** Stiffness vs. number of load cycles of an SLS-specimen with two  $\frac{1}{4}$ " CF-PEEK-fasteners, combined with the corresponding accumulated number of hits, accumulated AE-signals energy and single peak frequency

introduces a multi axial stress state into the fastener resulting in further bearing damages in the laminates.

During the 3rd stage (up to 80–90% of fatigue life) a continuous stiffness decrease is observed because of further damage in the fasteners. A propagation of the cracks in the head and the thread of the bolt can be analysed. Manufacturing imperfections strongly affect the failure process of the fasteners. Investigations on several different specimens showed an extensive crack propagation starting from and growing along fibre undulations. Especially damages in the countersunk head develop significantly in this stage. The countersunk head starts to shear at the point of the highest stresses, which can also be seen as a small crack near the top of the countersunk head. During the cyclic load test, the crack is growing in circumferential direction. Additionally, the bearing damage is propagating through the laminates. Kinking fibres, inter fibre cracks and delaminations between plies are detectable.

During the fatigue life, unexpected effects occurred for various number of specimens. In Fig. 19 is a showcase for such an event. At approximately  $7 \times 10^5$  cycles AE-events indicate increasing damage to the joint due to a 2% increase of the energy release rate of the AE-signal. Interestingly, the stiffness of the joint is slightly increasing in spite of occurring damages. It is assumed that due to the damage the joint deforms, which increases the load carrying area. The primary bending of the bolt and the secondary bending of the specimen lead to wedge the joint components. As a result, an increase of the stiffness of the joint is detectable.

The finale Stage 4 (> 99% of fatigue life) of the SLS-specimen is characterised by a rapid increase in detected AE-signals (compare Fig. 19). The accumulated energy release rate increases within only a few cycles. Peak frequencies between 400 and 800 kHz indicate fibre failure in the joint. A cut view at ~ 99% of the fatigue life in Fig. 20 reveals significant bearing damages in the laminate plates. Further, at the countersunk head shear failure (cracks) occurs

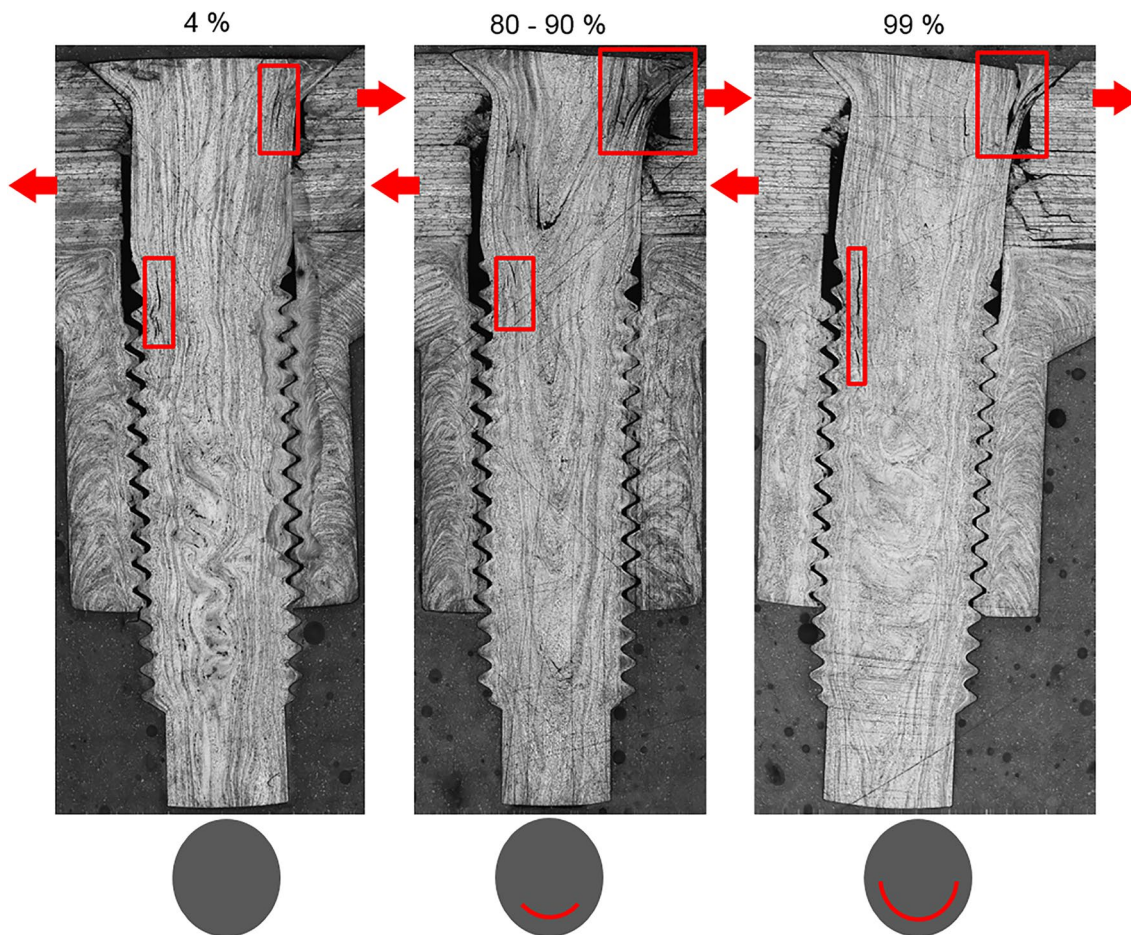


**Fig. 20** Failure mechanisms for 1/4" CF-PEEK-fasteners after 4% fatigue life: inter fibre fracture in shaft and thread, bearing damage, no damages on top of countersunk head. 80–90% fatigue life: propagation of inter fibre fracture in shaft and thread, bearing damage in

laminate, shear failure in the upper part of countersunk head. 99% fatigue life: propagation of inter fibre fracture in thread region, distinct bearing damage in laminate shear failure of countersunk head

which propagated over half of the bolt circumference. This failure mode leads to a larger deflection of the bolt, resulting in a further crack opening in the section of the thread and initiating the finale catastrophic failure.

Comparing the failure mechanisms occurring in the joints with CF-PEEK fastener due to quasi static and fatigue loading, it can be stated that the fibre orientation in the transition area from countersunk head to bolt shaft takes a distinct impact on the failure process. Inter fibre fractures in the countersunk head occur at an early stage of the fatigue life and grow with increasing numbers of loading cycles and effect, therefore, the performance of the bolt. The failure mechanisms which can be observed in the 3/16" CF-PEEK-fasteners are similar to those in the 1/4"-fasteners, which is inter fibre fracture near the thread and shear failure in the countersunk head. In addition, the 3/16"-fasteners exhibit a shear failure of the bolt in the contact area of the two laminate plates. Ti-fasteners fail due to a stress concentration in the first pitch of the thread in the bolt.

The microscopic cut views in Fig. 21a–c show the bearing damages in the laminate-plates of the specimen for all three tested joint configurations. Dominating failure modes are kinking fibres, inter fibre failure and varying degrees of delamination. Ultra-sonic C-scans show the size of the damage in the laminate after the finale failure of the SLS-joint in the cyclic load tests. The area of bearing damage for is determined by the ultrasonic c-scans using the area calculation tool in the freeware Infraview 4.32.

The area of the bearing damage in all three fastener configurations increases corresponding to fatigue life and the applied load on each specimen. For the 3/16" CFRP fastener the damaged area in the laminate is with 14.2 mm<sup>2</sup> the smallest. For the 1/4" CFRP and the 3/16" Ti-fastener an increase in the damaged area is detectable (see Fig. 21 c). The Ti-fasteners are exposed to the highest loads in the cyclic load test and show, therefore, the biggest damaged area.

Also the shear strength of the fastener and the resistance against deformation (shear modulus) have an impact on the size of the bearing damage. Comparing the two 3/16"-fastener systems, cut views indicate that for laminates mounted with a 3/16" CF-PEEK fastener chip outs and small delaminations only occur in the outer plies around the hole of the laminate plates. Whereas, joints mounted with 3/16" Ti-fasteners, delaminations and chip outs are visible over nearly the entire laminate thickness.

During cyclic loading wear in the contact area of the laminates occurred. The wear results from friction between the plates. The size of the wear area correlates with the clamping force introduced by the fastener into the joint and the number of load cycles. As expected, high number of load cycles and higher torques used for example in the 3/16" Ti-fastener, result in a larger abrasion zone around the borehole.

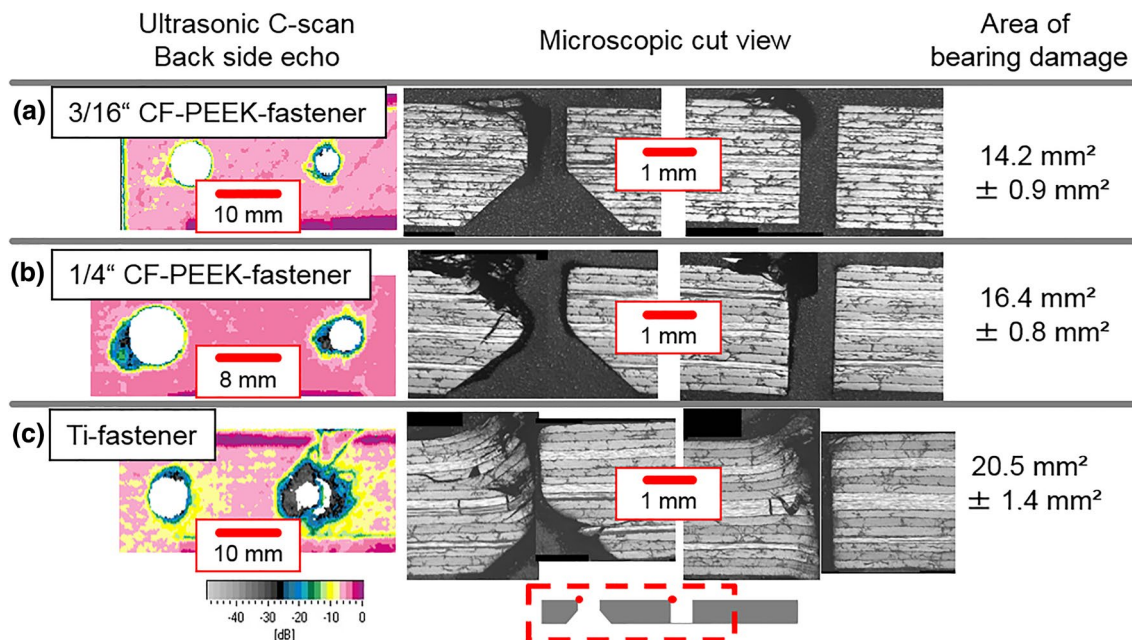
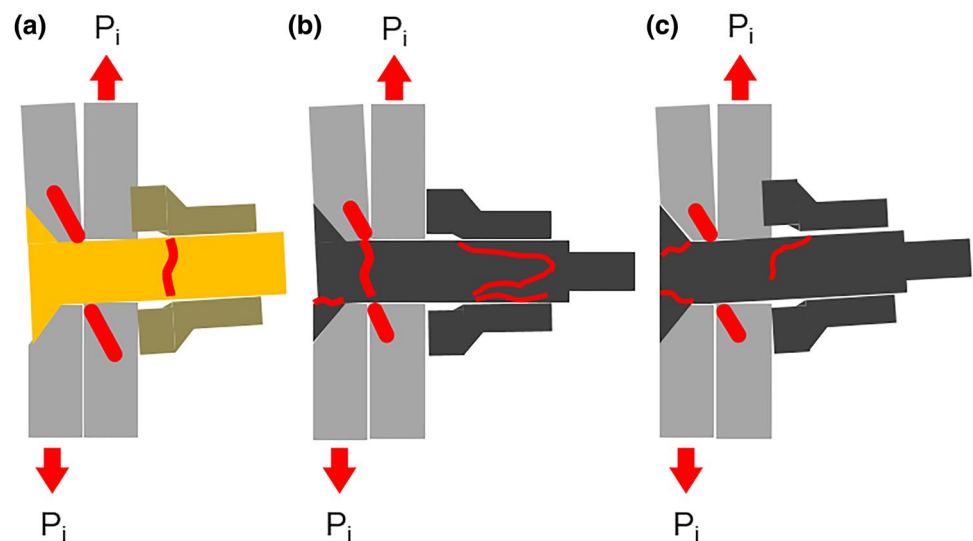


**Fig. 21** Bearing damage in one laminate plate for SLS-joint configurations, **a** specimen with 3/16" CF-PEEK-fastener, **b** specimen with 1/4" CF-PEEK-fastener, **c** specimen with 3/16" Ti-fastener; fasten-

ers not shown; damages in the laminates displayed with by back side echo of ultrasonic C-scan, microscopic 0°-cut views, and measured bearing damage area

**Fig. 22** Schematic illustration of the failure modes: **a** Ti-fastener: bearing damage in laminate and shear failure in the bolt. **b** 1/4" CF-PEEK-fastener: bearing damage in laminate, shear failure in the countersunk head and shaft. **c** 3/16" CF-PEEK-fastener: bearing damage in laminate and shear failure in the countersunk head



## 4 Summary

During the quasi-static test program, the finale failure of all specimens is a failure of the bolt. Different failure modes can be detected for each fastener system independent of parameter configurations of the SLS-specimens. In general it can be stated, Ti-bolts have higher load bearing capabilities than the CF-PEEK-fasteners of the same diameter. However, the 1/4" CF-PEEK-fasteners can bear comparable strength. Based on all tests carried out the following failure mechanisms can be summarized:

- Inter fibre fracture in the thread of the CFRP-bolt.
- Shear of the countersunk head of the CF-PEEK-fasteners.
- Ti-bolts always fail due to a stress concentration in the first pitch of the thread.
- Fibre and inter fibre failures in the CF-PEEK-fastener shaft within the cross section of the contact area of the two CFRP-plates.
- A combined load case of shear and tension on the CF-PEEK-fastener leads to the finale failure of the SLS-specimens.

In the laminate plates, bearing damage can be observed for each test (see Fig. 22). The bearing for the specimens tested with CF-PEEK-fasteners is smaller than with the Ti-bolts.

The enhanced analytical spring mass model describes the static behaviour of the different joint systems quite well and covers all variables influencing the joint behaviour. Different material properties and geometries can be calculated for the individual joint partners. On basis of the parameter variation, a deeper understanding of the impact of certain parameters is given on the model behaviour. By defining an expectancy range for the results of the calculation, a range

for the joint life can be given up to the damage initiation point. The analytical model thus supplies with little calculation effort a good fit of the results of loaded SLS-joint. Therefore, the model is a useful tool in planning and design of a bolted joint taking the parameters such as the fastener position, joint material, fastener type, hole diameter, joint thickness, bolt-hole clearance and bolt torque into account.

## 5 Conclusion

Based on the presented investigation of the failure process for different sets of SLS-test specimens in static and cyclic loading, several conclusions can be drawn. This study shows the high potential of the CF-PEEK-fastener especially in static tensile loading. The morphology of the fasteners take a sever influence on the failure process of the joint in fatigue loading. Therefore, a redesign of the CF-PEEK fastener regarding its geometry in relation to the fibre orientation within the bolt could increase the performance of the joint, since the current CF-PEEK fastener design can only have comparable performance with a Ti-bolts of one size smaller.

The developed enhanced analytical model is applicable for calculation of the joint behaviour in static loading, likewise for isotropic and anisotropic fasteners. Furthermore, the model describes the behaviour of a single-lap-shear joint with countersunk fasteners in more detail.

Employing acoustic emission during static and fatigue loading of the specimens, it is possible, using the accumulative energy of the signals in combination with the frequency spectrums, to describe the damage evaluation of the joint. Particular the degradation process in the fatigue lifetime for the joints can be displayed in detail.

**Acknowledgements** This work is funded by the German Ministry for Education and Research (BMBF) by a grant within “Spitzencluster Luftfahrt—Metropolregion Hamburg” (03CL34B).

## References

- Starikov, R.: Fatigue resistance of composite joints with countersunk composite and metal fasteners, (en). *Int. J. Fatigue* **24**(1), 39–47 (2002)
- Starikov, R., Schön, J.: Local fatigue behaviour of CFRP bolted joints. *Compos Sci Technol.* **62**(2), 243–253, (2002)
- Starikov, R., Schön, J.: Quasi-static behaviour of composite joints with countersunk composite and metal fasteners. *Compos. Part B Eng.* **32**(5), 401–411, (2001)
- McCarthy, M.A., McCarthy, C.T., Padhi, G.S.: A simple method for determining the effects of bolt–hole clearance on load distribution in single-column multi-bolt composite joints. *Compos. Struct.* **73**(1), 78–87, (2006)
- Stocchi, C., Robinson, P., Pinho, S.T.: A detailed finite element investigation of composite bolted joints with countersunk fasteners. *Compos Part A Appl. Sci. Manuf.* **52**, 143–150, (2013)
- Smith, P.A., Pascoe, K.J., Polak, C., Stroud, D.O.: The behaviour of single-lap bolted joints in CFRP laminates. *Compos. Struct.* **6**(1–3), 41–55, (1986)
- Ireman, T., Ranvik, T., Eriksson, I.: On damage development in mechanically fastened composite laminates. *Compos. Struct.* **49**(2), 151–171, (2000)
- Starikov, R., Schön, J.: Quasi-static behaviour of composite joints with protruding-head bolts. *Compos. Struct.* **51**(4), 411–425, (2001)
- Starikov, Roman: Quasi-static and fatigue behaviour of composite bolted joints. Royal Institute of Technology, Stockholm (2001)
- Smith, P.A., Pascoe, K.J.: Fatigue of bolted joints in (0/90) CFRP laminates. *Compos. Sci. Technol.* **29**(1), 45–69, (1987)
- Saunders, D.S., Galea, S.C., Deirmendjian, G.K.: The development of fatigue damage around fastener holes in thick graphite/epoxy composite laminates. *Composites* **24**(4), 309–321, (1993)
- Schuett, M., Wittich, H., Vernier, C., Nussbaeumer, F., Schulte, K., Investigation on the failure mechanisms of composite Fasteners with countersunk head in quasistatic and fatigue loading. In: ICCM 19 International Conference on Composite Materials, Montreal, (2013)
- Fiedler, B., Schütt, M., Wittich, H., Schulte, K., Investigation on the failure mechanisms of thermoplastic composites fasteners in single-lap shear joints under fatigue loading. In: 14th Japanese-European Symposium on Composite Materials, (2015)
- Schuett, M., Wittich, H., Nussbaeumer, F., Schulte, K., Fiedler, B., Investigation on the failure mechanism of composite fasteners with countersunk head in fatigue loading. In: ECCM 16 European Conference on Composite Materials, Seville (2014)
- Schürmann, H.: Konstruieren mit Faser-Kunststoff-Verbunden. (engl. Design with Fibre Reinforced Plastics), 2nd edn. Springer-Verlag, Berlin Heidelberg, (2007)
- McCarthy, C.T., Gray, P.J.: An analytical model for the prediction of load distribution in highly torqued multi-bolt composite joints. *Compos. Struct.* **93**(2), 287–298 (2011)
- Tate, M.B., Rosenfeld, S.J., Preliminary Investigation of the Loads Carried by Individual Bolts in Bolted Joints: National Advisory Committee for Aeronautics, 1946
- Nelson, W.D., Bunin, B.L., Hart-Smith, L.J.: Critical joints in large composite aircraft structure. In: Douglas Aircraft Co, Inc, Long Beach, CA, United States NASA-CR-3710, NAS 1.26:3710, DP-7266, 1983
- Barrois, W.: Stresses and displacements due to load transfer by fasteners in structural assemblies. *Eng. Fract. Mech.* **10**(1), 115–176, (1978)
- Liu, F., Zhang, J., Zhao, L., Xin, A., Zhou, L.: An analytical joint stiffness model for load transfer analysis in highly torqued multi-bolt composite joints with clearances. *Compos. Struct.* **131**, 625–636, (2015)
- Olmedo, C., Santiuste, Barbero, E.: An analytical model for the secondary bending prediction in single-lap composite bolted-joints. *Compos. Struct.* **111**, 354–361, (2014)
- Hart-Smith, L.J., Mechanically-fastened joints for advanced composites—phenomenological considerations and simple analyses. In: Lenoe E., Oplinger D., Burke J., (eds.) *Fibrous composites in structural design.*, pp. 543–574. Springer, New York, (1980)
- Ekh, J., Schön, J.: Load transfer in multirow, single shear, composite-to-aluminium lap joints. *Compos. Struct.* **66**(7–8), 875–885, (2006)
- Ireman, T.: Three-dimensional stress analysis of bolted single-lap composite joints. *Compos. Struct.* **43**(3), 195–216, (1998)
- Egan, B., McCarthy, C.T., McCarthy, M.A., Frizzell, R.M.: Stress analysis of single-bolt, single-lap, countersunk composite joints with variable bolt-hole clearance. *Compos. Struct.* **94**(3), 1038–1051, (2012)
- Gutkin, R., Green, C.J., Vangrattanachai, S., Pinho, S.T., Robinson, P., Curtis, P.T.: On acoustic emission for failure investigation in CFRP: Pattern recognition and peak frequency analyses. *Mech. Syst. Signal Process.* **25**, (4), 1393–1407, (2011)
- Radmeier, M., Jahnke, P., Meyer, H., Grosse, C., Failure mechanisms of carbon-fiber-reinforced polymer materials characterized by acoustic emission techniques. In: 30th European Conference on Acoustic Emission Testing and 7th International Conference on Acoustic Emission, University of Granada, (2012)
- Berthelot, J.M., Rhazi, J.: Acoustic emission in carbon fibre composites. *Compos. Sci. Technol.* **37**(4), 411–428, (1990)
- Paget, C.A., Delamination Location and Size by Modified Acoustic Emission on Cross-ply CFRP Laminates during Compression-Compression Fatigue Loading. In: ICCM-17 17th International Conference on Composite Materials, Edinburgh, 2009
- Qi, G.: Wavelet-based AE characterization of composite materials. *NDT & E Int.* **33**(3), 133–144, (2000)
- Surgeon, M., Wevers, M.: Modal analysis of acoustic emission signals from CFRP laminates. *NDT & E Int.* **32**(6), 311–322, (1999)
- D5961\_D5961M, Test Method for Bearing Response of Polymer Matrix Composite Laminates: ASTM International, D30 Committee. West Conshohocken, PA
- Mense, L., Schmid, S., Hintze, W., Clausen, R., Schütte, C., Dose, F., Süess, B.: “Bohrwerkzeug”, Deutschland 10 2010 012 963, September 29, 2011
- Ed, E.T.H., Das Composite-Fliesspressen: Ein neues Verfahren zur Net-Shape-Fertigung von Endlosfaserverstärkten Bauteilen mit thermoplastischer Matrix dargestellt am Beispiel einer Schraube für die Translaminäre Wirbelfixation. Abhandlung zur Erlangung des Titels Doktor der Technischen Wissenschaften, (2001)
- Togini, G.T.R.: Höchsthochste Verbindungselemente aus endlosfaserverstärkten Verbundwerkstoffen mit thermoplastischer Matrix. Schraubenverbindungen (de)
- Togini, R.R., Turlach, G., Eds, Auslegung von höchstfesten Verbindungselementen aus endlosfaserverstärkten Thermoplasten: Schraubenverbindungen—Berechnungen, Gestaltung, Anwendung. VDI-Bericht, (2005)
- Decker: Maschinenelemente: Funktion, Gestaltung und Berechnung, 18th edn. Hanser Verlag, München (2011)
- Wittel, H., Muhs, D., Jannasch, D., Voßiek, J.: Roloff/Matek Maschinenelemente: Normung, Berechnung, Gestaltung, 22nd edn. Springer Vieweg, Wiesbaden (2015)

39. ASTM D3039/D3039M-11, Standard Test Method for Tensile Properties of Polymer Matrix Composite Materials, ASTM International, 2011. West Conshohocken, (2011)
40. ASTM D6641/ D6641M-11. In: Standard Test Method for Compressive Properties of Polymer Matrix Composite Materials Using a Combined Loading Compression (CLC) Test Fixture. ASTM International, West Conshohocken, (2011)
41. Schoßig, M.: (engl. Damage mechanisms in fiber-reinforced plastics: quasistatic and dynamic investigations). In: Schädigungsmechanismen in faserverstärkten Kunststoffen: Quasistatische und dynamische Untersuchungen. Vieweg + Teubner Verlag/Springer Fachmedien Wiesbaden, Wiesbaden, (2011)
42. Cole, R.T., Bateh, E.J., Potter, J.: Fasteners for composite structures. *Composites*, 13(3), 233–240, (1982)
43. Schulte, K., Fiedler, B., Structure and properties of composite materials. 2nd Edition. Hamburg, 2010